Acknowledgements

I would like to thank the following people:

Dr. Philip Perry for his guidance, support and patience throughout this project.

Gareth, Kevin, Muggy, Marie, Declan and all my family in Donegal.

Declaration

I hereby certify that this material, which I now submit for assessment on the programmme of study leading to the award of Masters in Electronic Engineering is entirely my own work and has not been taken from the work of others save to the extent that such work has been cited and acknowledged within the text of my work.

Signed: Paul Sheridan Date: 21/12/99

Contents

List of Figures

List of Tables

Abstract

Prediction and Reduction of Third-Order IMD in Multichannel Amplifiers

Submitted by: P. Sheridan

The advent of the multichannel amplifer (MCA) has brought with it strigent intermodulation distortion (IMD) requirements. This thesis explores the issue of third-order intermodulation distortion (IM_3) in MCA's from two seperate viewpoints.

Firstly, the prediction of IM_3 levels in MCA's is investigated and a novel software based prediction tool is presented. The amplifier is viewed as a black-box nonlinear circuit and is characterised by carrying out an IMD test using 3 tones of equal amplitude. Then, by using the Volterra-series approach and linear interpolation, an IM_3 prediction can be made for an arbitrary number of input tones of different amplitudes. To demonstrate and verify the capability of this technique predicted and measured results are compared for single and cascaded stages.

Secondly and finally, a novel amplifier configuration which reduces these IM_3 levels and simultaneously improves the overall efficiency of the MCA is presented. This approach uses a scaled version of the extracted envelope of the mult-tone signal to actively bias the amplifier. This technique is of paramount importance in multi-channel power amplifier (MCPA) design where an increase in linearity is usually achieved by a decrease in efficiency. Practical results are presented which illustrate the effectiveness of this technique.

Chapter 1

Introduction

1.1 Market Review

The largest telecommunications growth area in recent years is in mobile telephony. At the end of 1997 there were about 207 million mobile telephony subscribers worldwide, an increase of more than 70 million during 1997 alone. By the end of 2001 there will be an expected 605 million users worldwide. As confirmation of this trend, more individuals signed up for mobile telephone services than fixed services in 1997 [1]. In parallel with this growth there will be an expected 575 million Internet users by the year 2001 [2]. The next significant step in wireless communications will be linking the two together adding a considerable range of new and more advanced services involving high speed data, video and multimedia communications on a global scale. This is the basis for what is known as the third-generation mobile phone service. It is expected that early demands will come from the business community and, as with the mobile phone, this will quickly evolve into mass-market services.

At present, the world of terrestrial digital mobile communications is actually three worlds that are not compatible. Europe gave the world the Global System for Mobile Communications (GSM) standard. USA use the Advanced Mobile Phone System (AMPS) standard, it's digital derivative D-AMPS and the spread spectrum system. These standards are widely employed around the world but unfortunately, despite

the fact that they are based on the same radio technology, they are not compatible. Meanwhile, Japan selected yet another standard, called Personal Digital Cellular (PDC), which is used only within Japan.

Cellular systems aside, a standard for cordless and low tier wireless local loop (WLL) telephony called DECT (Digital Enhanced Cordless Telephony) has expanded on a global scale. DECT may also have a significant part to play in third-generation services. According to recent research by KPMG, a UK-based consulting group, it is in conjunction with GSM and other cellular standards that DECT will enjoy the most success due to it's frequency efficiency [3].

These are the terrestrial (earth-based) wireless standards. There is, of course, yet another dimension to wireless networks in the shape of satellite-based mobile communication services. Even when coverage of cellular mobile networks is complete, they will only cover 20 percent of the earth's surface. Areas, such as deserts, with very low population densities mean it will never be economic to install a cellular infrastructure. This is where satellite-based services will fit in as they provide good coverage over very large areas.

As may be evident from the above discussion, the entire telecommunication world is based on technical standards that define how various pieces of equipment communicate with each other. In wireless communication systems, a new set of common standards is required to permit third-generation sevices to be offered. In Europe, the European Telecommunication Standards Institue (ETSI) promotes this global standardisation process by co-ordinating it's activities with international standardisation bodies, such as the International Telecommunications Union (ITU). In January 1998, ETSI announced that it has selected GSM as the core network standard and WCDMA (Wideband Code Division Multiple Access) [4] as the main technology for third-generation UMTS (Universal Mobile Telecommunications System) that will be introduced throughout the EU.

A major limiting factor in the development of third-generation systems is bandwith at the air interface which limits the volume of information that can be transmitted between the wireless terminal and the network. As well as this, merging voice and

data will significantly increase the cost and complexity of the network. In recent years there has been a significant amount of research to tackle these problems and one of the most successful developments has been the development of systems which use multiple carrier or multichannel architectures.

1.2 Multichannel Amplifiers

Traditionally, many wireless system applications (*e.g.*, satellite systems and cellular base-stations) relied on the high-level combination of individual single-channel amplifiers. As the number of channels grows, this approach becomes hardware-intensive, bulky and costly. As a result, the high-level combining of multiple amplifiers has been supplanted by a single multichannel amplifier (MCA) in an increasing number of systems. Almost all modern mobile communication sytems (*e.g.*, cellular, satellite and DECT) use MCAs along with other systems such as MMDS (Multichannel Multipoint Distribution System), LMDS (Local Multipoint Distribution System) and MVDS (Microwave Video Distribution System) which are either in service or advanced stages of development. MMDS, LMDS and MVDS are broadband wireless access systems developed for the delivery of television signals, Internet access and interactive multimedia sevices such as video on demand [5]. Evolving high data rate broadband ATM systems will also use MCAs [6].

MCAs eliminate the need for additional hardware and thus reduce the system's complexity and size as well as offering complete flexibility in the assignment of channels [8]. The advent of the MCA has brought with it stringent performance requirements. A primary performance criterion is linearity; the input-output relationship must have low intermodulation distortion (IMD) levels in order to preserve signal integrity. When multiple signals are transmitted through an amplifier additional and unwanted frequency components are generated at the output due to IMD. Similar problems are also evident in multichannel receivers as the IMD's reduce the spur-free dynamic range of the system. The IM products of greatest concern are usually of the third-order type as they occur closest to the carriers that generate them and are the strongest.

This thesis explores the IMD problem in MCA's from two seperate viewpoints. Firstly, the prediction of third-order IMD (IM_3) levels in MCA's is investigated and a software based prediction tool is developed. This will be of considerable use in RF system design as IM_3 predictions for single and cascaded stages are made possible. Secondly and finally, a novel amplifier configuration which reduces these IM_3 levels and simultaneously improves the overall efficency of the MCA is presented. This technique is of paramount importance for multichannel power amplifier (MCPA) design where an increase in linearity is usually achieved by a decrease in efficiency [9][10]. Practical amplifier measurements will be used for verification purposes throughout this thesis.

1.3 Thesis Structure

This thesis is organised into two seperate sections preceeded by a general introduction to the fundamental concepts. The first section, Chapters 3 through 6, is devoted to the characterisation and prediction of third-order IMD levels in MCA's and is the larger of the two sections. The second part, contained in Chapter 7, presents a novel amplifier configuration which is shown to reduce these IM_3 levels and simultaneously improve the overall amplifier efficiency.

Chapter 2 details the fundamental concepts of this thesis. Important amplifier performance specifications are defined and explained. A contrast between linear and nonlinear systems is given and the output characteristics of both types of systems are explained. The concept of a weakly nonlinear system is explained along with an introduction to intermodulation distortion. It concludes with an overview of the efficiency and linearity requiements in multichannel power amplifiers.

In Chapter 3 practical measurements of IM_3 levels in three different MCA's are taken. The standard two-tone test is first implemented and then the measurement system architecture is extended to allow for a three-tone (multi-tone) test set. In order to obtain a complete amplifier characterisation a software routine incorporating a GPIB interface is used. This enables control of the multi-tone excitation levels

along with the capture and retrieval of IM_3 data. The retrieved data is used at a later stage for the evaluation of the IM_3 prediction software.

The nonlinear analysis technique, called the Volterra Series Approach, that is employed here is presented in Chapter 4. The Volterra Series, or nonlinear transfer function approach, is widely accepted as an effective means of characterising weakly nonlinear circuits having multi-tone excitation [12][16]. The MCA's considered here are perfect examples of such circuits.

Chapter 5 contains the design and development methodologies for the Volterra based prediction tool. Initially, a three-tone prediction routine is developed. Following this, a multi-tone (greater than 3) prediction routine is developed which can generate IM_3 predictions for single and cascaded stages.

An evaluation of the software based prediction tool is carried out in Chapter 6. To demonstrate and verify the capability of this technique a comparison between predicted and measured results (from Chapter 3) for a selection of single and cascaded silicon BJT MCA stages is given.

The second part of this thesis is contained in Chapter 7. The conflicting performance requirements, linearity and efficiency, in mutlichannel power amplifiers are discussed. Existing techniques of improving on both of these requirements are investigated. A novel amplifier configuration which deviates from previous methods is then presented. The technique uses a scaled version of the extracted envelope of the multi-tone signal to actively bias the amplifier thus ensuring a low level of power consumption and minimal IMD levels.

A performance evaluation of the amplifier configuration is then conducted. For verification purposes the MCPA can be switched from it's "normal" bias configuration, a simple collector feedback circuit, to the active bias configuration described here. Measurements of worst case adjacent channel IMD levels and amplifier efficiency are taken for both biasing schemes and compared.

Chapter 8 gives conlusions and makes recommendations for future developments on both parts of the thesis.

Chapter 2

Fundamental Concepts

2.1 Amplifier Performance Characteristics

An amplifier can be specified in terms of it's gain, 1-dB compression point, noise figure and spurious-free dynamic range. Some of these specifications will be more applicable to an amplifier than others depending on the purpose of the amplifier. Each of these performance requirements will now be defined:

Gain The amplifier power gain (G) is defined as the ratio of output power (P_{so}), in watts, to available input signal power (P_{si}), in watts, as follows

$$G = \frac{P_{so}}{P_{si}} \tag{2.1}$$

and can be defined in dB as follows

$$G(dB) = 10log_{10}(G) \tag{2.2}$$

In terms of S-parameters the power gain is often expressed as $G = \mid S_{21} \mid^2$. This gain will only be realised if the amplifier is perfectly matched and inserted between a matched load and a matched source [7]. Since this scenario rarely occurs, it is necessary to define the gain which will be exhibited between arbitrary impedances. This is sometimes called the insertion gain or, more commonly, the transducer power gain.

1-dB Compression Point The 1-dB compression refers to the power level at which the actual output power drops 1 dB below the linearly predicted power. Figure 2.1 gives a visual representation of the 1-dB compression point.

Noise Figure The noise figure (NF), in dB, describes the deterioration of the signal-to-noise ratio due to the presence of an amplifier. It is defined as follows:

$$NF(dB) = 10log(\frac{P_{si}/P_{ni}}{P_{so}/P_{no}}) \tag{2.3}$$

where P_{ni} is the available input noise power, in watts, and P_{no} is the available output noise power, in watts. P_{si} and P_{so} are defined as the available input and output signal powers respectively.

Spurious-Free Dynamic Range The spurious-free dynamic range is the ratio of the maximum distortionless input signal to the minimum detectable signal. The minimum detectable signal is determined by the noise generated by the amplifier. Figure 2.1 illustrates the spurious-free dynamic range along with the other performance characteristics.

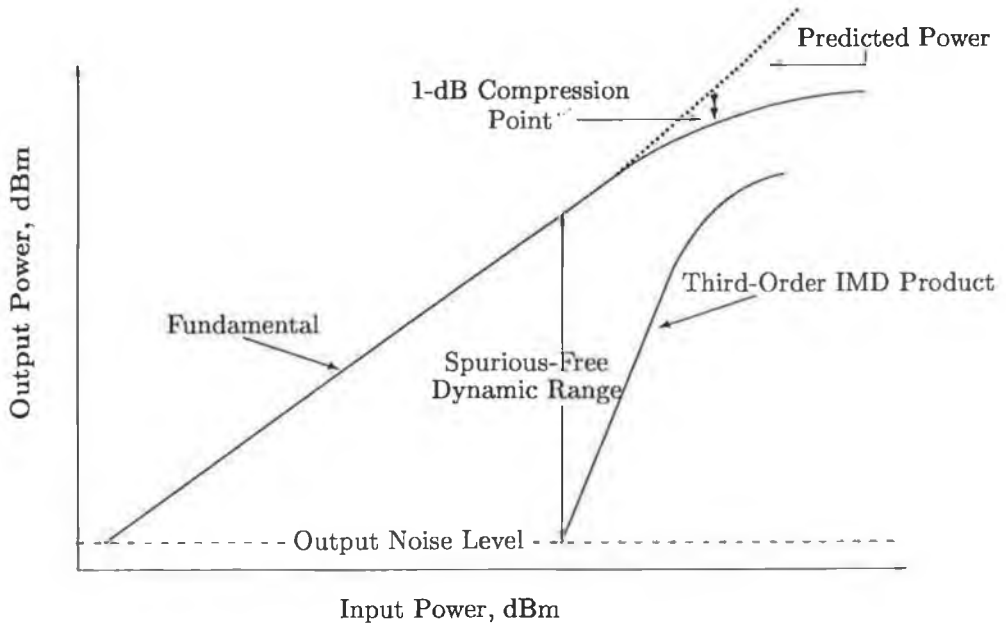

Figure 2.1: Performance characteristics for a typical amplifer

2.2 Linearity and Nonlinearity

It is well known that in the real world the term "linear amplifier" is an approximate, and sometimes optimistic term. All active devices have measurable nonlinearity at any point of their useful operating range [11]. In active devices, nonlinearities are responsible for phenomena, such as IMD, that degrade system performance and for this reason cannot be ignored. Linear circuits or systems are defined as those for which the superposition and proportionality principles hold [12]. Formally, suppose a system takes an input $x(t)$ and produces an output $y(t)$ via some function f,

$$y(t) = f[x(t)] \tag{2.4}$$

where t is an independent variable, usually time. Suppose futher that two inputs $x_1(t)$ and $x_2(t)$ produce outputs $y_1(t)$ and $y_2(t)$, respectively:

$$y_1(t) = f[x_1(t)] \tag{2.5}$$

$$y_2(t) = f[x_2(t)] \tag{2.6}$$

Then, if the system is linear, superposition and proportionality may be applied, so that an input $ax_1(t) + bx_2(t)$ will produce an output $ay_1(t) + by_2(t)$, where a and b are scalars. That is,

$$ay_1(t) + by_2(t) = f[ax_1(t) + bx_2(t)] \tag{2.7}$$

for a linear system.

Many systems that are decribed as linear also hold the property of being time-invariant. A system is time-invariant if a time shift in the input is reproduced at the output. Suppose

$$y(t) = f[x(t)] \tag{2.8}$$

Let T_0 be a constant. Then, for all values of T_0,

$$y(t - T_0) = f[x(t) - T_0] \tag{2.9}$$

in a time-invariant system. A system is time-varying if it is not time-invariant.

To put it another way, in a linear time-invariant system the frequency content at the output is always identical to that of the input. This is not true with nonlinear systems which generate new frequency components at their output [16].

Nonlinear circuits are usually characterised as either strongly nonlinear or weakly nonlinear. Strong nonlinearities are characterised by abrupt changes within the operating regions of their characteristics, for example, a strongly driven transistor. These circuits are not of interest here and will no longer be discussed. On the other hand, weak nonlinearities lack abrupt changes within the operating regions of their characteristics; their input-output relationships vary gradually as a function of the input amplitude. Many weakly nonlinear circuits, such as the MCA's considered here, generate distortion products that are great enough to be of concern [12].

2.2.1 Intermodulation Distortion

Intermodulation distortion, as it's name implies, is the presence of unwanted signals that have been created by mixing action (modulation) among two or more signals in nonlinear circuits [13]. IMD products generated in an amplifier or receiver often present a very serious problem, because they represent spurious signals that interfere with, and can be mistaken for, desired signals.

For example, consider an amplifier having only quadratic and cubic nonlinearities. A power series expansion can then be used to model the weak nonlinearities as follows:

$$V_o = a_1 V_i + a_2 V_i^2 + a_3 V_i^3 \tag{2.10}$$

where V_i is the input signal and V_o is the corresponding output signal. Let the amplifier input signal consist of two equal amplitude sinusoidal signals at frequencies f_1 and f_2 respectively, where f_2 is greater than f_1:

$$V_i = V\cos(2\pi f_1 t) + V\cos(2\pi f_2 t) \tag{2.11}$$

Substituting (2.11) into (2.10) and using the appropriate trigonometric identities readily shows that the output contains an array of intermodulation products. Appendix A gives the complete mathematical expansion. Figure 2.2 shows the spectrum of frequency components at the amplifier's input and output. The terms marked (1) indicate components resulting from the linear behaviour of the amplifier. Terms that are generated by the quadratic and cubic nonlinearities are marked (2) and (3), respectively. It can be seen that the second-order IM products occur at frequencies

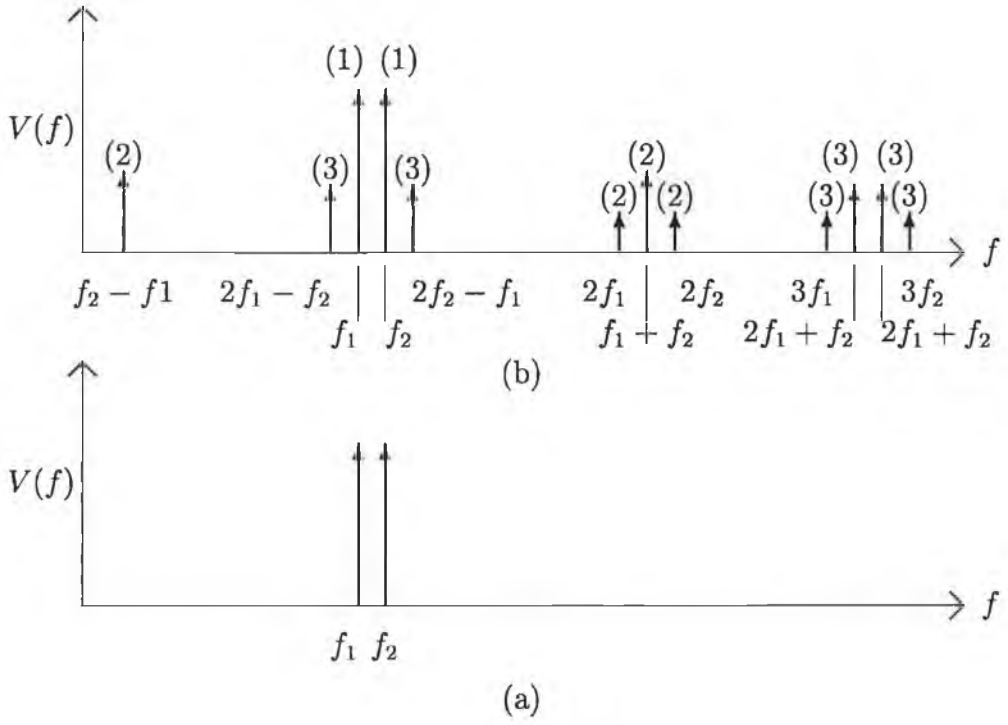

Figure 2.2: Intermodulation distortion in an amplifier with quadratic and cubic nonlinearities.(a)Frequency content at input. (b) Frequency content at output.

well above and below the signals that generate them and consequently are of little concern. In general, this is true for all even-order IM products. As stated earlier, the IM products of greatest concern are of the third-order type as they occur closest to the signals that generate them, as illustrated in Figure 2.2. The IM_3 products are also the strongest of all odd-order products and have the same separation from the input carriers as the separation of the carriers themselves and therefore cannot be filtered out, showing up as either co-channel or adjacent channel interfering signals. Consider, for example, a MCA used in cellular base station applications. This type of amplifier has many independant carriers with equal frequency seperation and therefore undesired IM_3 products will be generated inside other channel's bandwidth.

2.3 Efficiency and Linearity Requirements in MCPA's

Current commmunication system trends have provided a requirement for highly linear multichannel power amplifier's (MCPA's) with low power consumption or high efficiency. For example, in digital mobile radio and satellite systems intensive research is being carried out to develop new techniques that allow MCPA's to meet these performance requirements [14].

Efficiency, denoted η, is defined as the ratio of RF output power to DC input power. An expression for overall efficiency is given by

$$\eta = \frac{P_{os} - P_{is}}{P_{dc}} \tag{2.12}$$

where P_{dc} is the power supplied to the amplifier by it's power supply [15]. In MCPA's high efficiency is usually achieved by a decrease in the device's linearity performance. Therefore, design techniques that improve both linearity and efficiency in MCPA's are of great importance. The fundamental concepts of IMD in MCA's have already been introduced in Section 2.2.1.

Chapter 3

Intermodulation Measurement System

3.1 Introduction

In order to obtain a complete picture of IM_3 behaviour in MCA's, prior to developing a prediction tool, a practical third-order IMD measurement system is required. The measurement system is designed in a robust manner so that a complete measurement of the output spectrum for a selection of MCA's can be carried out. MCA's used in most modern communications receivers seldomly receive multiple signals of equal power side by side. To depict this feature in the measurement system, the input tones are assigned a range of power levels below the 1-dB gain compression point for varied channel spacings. This task performed manually would prove laborious and time consuming and therefore it is desirable to perform the measurement in a software enviroment.

3.2 Multi-tone Characterisation of Amplifiers

As the distortion products of interest here are third-order it is possible to characterise the multi-tone ($Q \geq 3$) performance based on measurements using only three tones,

where Q is the number of excitation tones. Firstly, consider the case where $Q = 3$ and the three equally spaced excitation tones are given by f_1, f_2 and f_3. The IM_3 components generated are of two types: those generated from two-tone IMD

$$\begin{aligned} f_{IM} &= 2f_1 - f_2 \quad \text{and} \quad 2f_2 - f_1 \\ &\text{and} \quad 2f_2 - f_3 \quad \text{and} \quad 2f_3 - f_2 \\ &\text{and} \quad 2f_1 - f_3 \quad \text{and} \quad 2f_3 - f_1 \end{aligned} \tag{3.1}$$

and those generated from three-tone IMD

$$\begin{aligned} f_{IM} &= f_2 + f_1 - f_3 \\ &\text{and} \quad f_1 + f_3 - f_2 \\ &\text{and} \quad f_2 + f_3 - f_1. \end{aligned} \tag{3.2}$$

In order to detect and measure all of the IM_3 components generated it is necessary to slightly offset one of the tones in frequency as some of the components fall at the same frequency as other components or excitation tones. The frequency offset distance is limited by the resolution characteristics of the spectrum analyser. The frequency resolution is determined by the bandwidth and the shape factor of the last IF filter (last filter before detection) and the sideband noise of the spectrum analyser. The IF bandwidth, or resolution bandwidth (RBW), is normally specified in terms of its 3-dB bandwidth. A narrower IF bandwidth provides better resolution but imposes a limit on the sweep time [7]. For example, if an analyser has its narrowest IF bandwidth as 1 kHz, the closest any two signals can be and still be resolved (or seen on the SA) is 1 kHz.

When measuring closely spaced frequency components of unequal amplitude, the characteristic of the filter shape is also important. The filter shape is normally characterised by ratio of $\Delta f_{60dB}/\Delta f_{3dB}$ (the 60-dB to 3-dB bandwidth), which is known as the IF shape factor [7]. The smaller the shape factor, the greater the analyser's capability to resolve closely spaced signals of unequal amplitude. If, for example, the shape factor of a filter is 15:1, then two signals whose amplitudes differ by 60 dB must differ in frequency by 7.5 times the IF bandwidth before they can be successfully measured. Otherwise the signals become distorted and the accuracy of the amplitude measurement is reduced [17].

In conjunction with resolution there are a number of other parameters to be considered when using a spectrum analyser for IMD measurements such as frequency range, dynamic range, video bandwidth (VBW) and noise. The frequency range of the spectrum analyser should, obviously, cover the measurement range. The dynamic range, as it applies to a spectrum analyser, is defined as the ratio of the largest signal to the smallest signal that can be displayed simultaneously without analyser distortion products. Also, the spectrum analyser can be used to measure the noise associated with a signal provided the noise power is higher than the noise floor of the analyser at a particular resolution bandwidth (RBW). The video filter is a post-detection lowpass filter used before feeding the detected signal to the display. The VBW is usually much less than the RBW and gives an average value of the noise signal.

The complete set of IM_3 components generated from IMD involving three tones of equal amplitude is shown in Figure 3.1. For the more general case, where $Q \geq 3$, the IM_3 components are still generated from mixing action involving a maximum of three tones. Now, for Q equally spaced excitation tones given by $f_1, f_2, \ldots, f_Q$ the IM_3 components generated are, again, of two types: those generated from two-tone IMD

$$f_{IM} = 2f_n - f_m \quad \text{and} \quad 2f_m - f_n \tag{3.3}$$

and those generated from three-tone IMD

$$\begin{aligned} f_{IM} &= f_m + f_n - f_l \\ &\text{and} \quad f_n + f_l - f_m \\ &\text{and} \quad f_m + f_l - f_n. \end{aligned} \tag{3.4}$$

3.3 Measurement System Architecture

The standard test set-up for IM_3 measurements involves generating two equal power signals, f_1 and f_2, separated by a specified fequency, $\Delta f = f_2 - f_1$, and measuring the resultant IM_3 products, $2f_1 - f_2$ and $2f_2 - f_1$. As explained in Section 3.2,

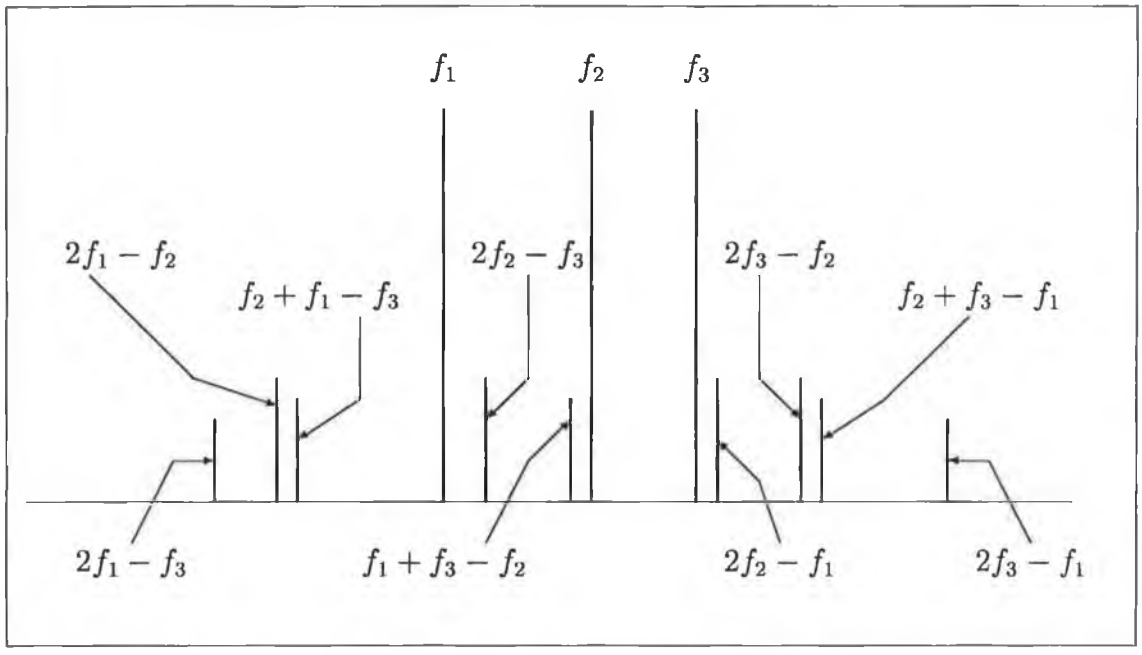

Figure 3.1: Third-order IMD components generated by 3 tones of equal amplitude.

when $Q \geq 3$ IM_3 components are generated from both two-tone and three-tone IMD which means that the standard two-tone test set-up is no longer adequate. However, a similar type measurement arrangement can be used for the multi-tone case with the inclusion of a third signal source. The set-up, shown in Figure 3.2, consists of three signal generators, a combiner, the necessary connections to the device under test and a spectrum analyser to detect and measure the distortion products. A PC installed with GPIB software is used to control the signal generator output power level and frequency as well as the capture and retrieval of IM_3 levels from the spectrum analyser (SA). The PC is connected to the signal generators and SA in a daisy chain arrangement.

3.4 Measurement System Accuracy

Although the arrangement is very straightforward, there are several important guidelines that must be followed to ensure accurate measurement [13][18][19][20] . Firstly, the signal sources must be stable and accurate in frequency, with very low noise to

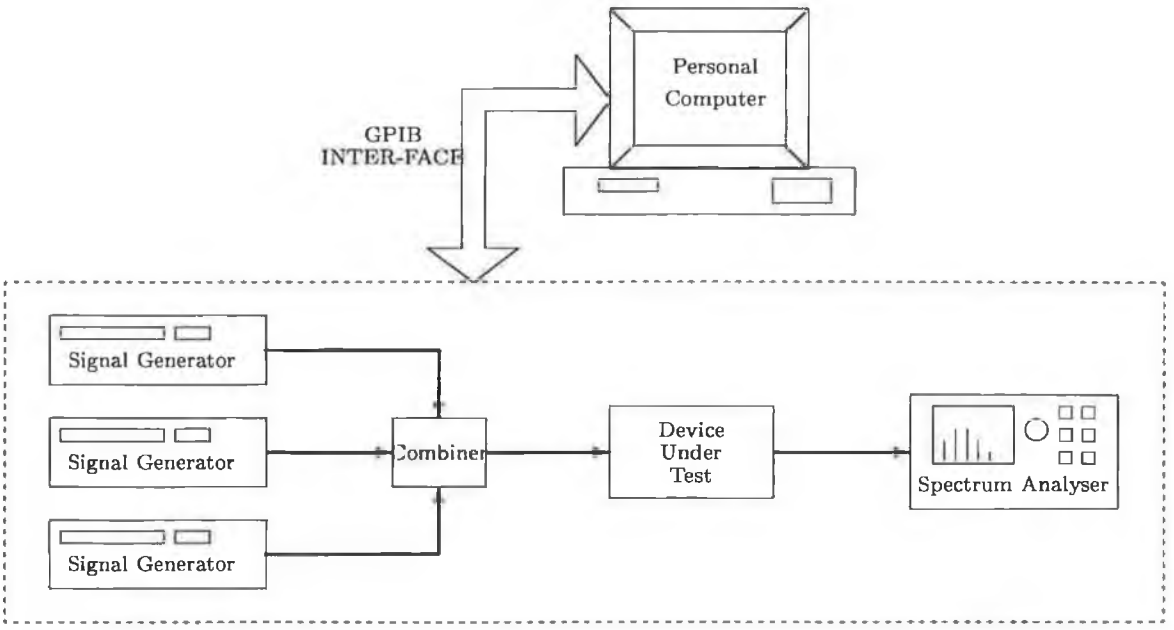

Figure 3.2: Block Diagram of IM_3 Measurement System.

avoid ambiguity when measuring very low levels of IMD. The three synthesised signal generators used here, two Anritsu and one HP, are externally phase locked to a common reference oscillator to ensure precision frequency offsets between the carriers. Also, the output power levels of the signal sources must be closely matched in amplitude initially to avoid variations due to the measurement set-up. Unequal amplitude sources will create unequal amplitude IMD products; this is undesirable as the purpose of the system is to measure the effects of the device under test, rather than the characteristics of the instrumentation.

The combiner circuit must be chosen so as not to generate significant distortion and also to provide good isolation between the three signal sources. The Mini-Circuits MA3PD-2 3-1 passive combiner circuit used here provides adequate isolation and low distortion for the range of power levels considered here. Finally, the spectrum analyser must not contribute errors to the test results from internal distortion in the instrument. Again, for the Anritsu MS2651A and the low power levels used here this should not be a problem. In the case of larger input signal levels the spectrum analyser's input circuits may become overloaded creating a new set of distortion products that can confuse or even obscure the desired measurement. A typical test

for internal distortion in a SA is to attenuate the input of the analyser by 10 dB and to check that the measured results also change by 10 dB. This was the case in all measurements made.

3.5 Measurement Procedure

3.5.1 Introduction to Software Development

The general hardware to software interface for the measurement system has already been introduced in Section 3.3. The software program used to carry out all interactions with the measurement instrumentation will now be discussed. As the GPIB software package [21] is compatible with the C Programming Language [23], the entire routine can be implemented in C.

3.5.2 GPIB Software

The GPIB software is directly responsible for the control of the measurement hardware as well as the capture and recovery of the required data. It consists of two linked entities, namely, the GPIB software routines, which are responsible for the general interaction with the measurement instrumentation and the inherent GPIB command codes specific to each instrument. The GPIB software consists of a set of programming libraries for the C language. These libraries consist of many different routines which allow extensive control of the GPIB bus. The basic routines used in the computer-controller program to enable interaction which each instrument in the measurement system are IBFIND, IBWRT and IBRD. These are used to capture an address, write to an address and read from an address respectively.

Before communication can take place between an instrument and the PC, the instrument must be captured by the PC via the GPIB bus. This is acheived by means of an IBFIND routine. Once the instrument has been captured, GPIB command codes can be used to request specific instrument responses using the IBWRT routine

[22]. For example, for the purpose of taking a reading of the SA marker level, the IBWRT routine is used in conjunction with the SA command code to output the marker level (MKR?). Having requested the data from the SA, an IBRD routine is then used to read this data back to the PC. Figure 3.3 details the basic GPIB routines and command codes used to return the marker level from the SA.

DEVICE = IBFIND(device name);	Captures the device (SA)
IBWRT(DEVICE, MKR?, cmd_length);	Requests marker level value
IBRD(DEVICE, BUFFER, buff_size);	Reads the data into a buffer.

Figure 3.3: GPIB instructions and command codes used to return the SA marker level.

3.5.3 Program Description

The C program responsible for the complete implementation of the measurement routine is described here. Figure 3.4 displays a flowchart for the overall program operation. The program is sectioned into routines and subroutines which are called at various stages upon execution. The INITIALISE function is called by the program firstly. This function initiates communication with the system devices (spectrum analyser and signal generators) through the GPIB bus using device names set up in the Computer Boards configuration program [21] and the IBFIND routine. Using IBWRT, the spectrum analyser and signal generators are then sent configuration commands to allow an IM_3 measurement for equally spaced tones to be carried out.

It should be noted that the configuration parameters can be set in the program prior to execution to enable measurement of different MCA's.

The MEASURE1 function is called next to initiate the actual measurement process. Control is passed to the Level_Adjust1 subroutine which adjusts the signal generators output levels. Using nested loops and counters the output levels (device input levels) are varied within a pre-designated range. The range is selected so that the MCA will always be operating below it's 1-dB compression point (in the linear region). After each adjustment to the signal level the Mkr_Read1 function is called to control the SA marker position and read its value back into an array. When the full set of measurements have been acquired and stored in arrays the control is passed back to the MEASURE1 function which completes the process by passing the stored array data in an output file. The signal generators various output levels are also stored in another data file. The complete measurement process is then repeated for the frequency offset case (to obtain all IM_3 components) with the measured results again stored in arrays and finally outputed to a data file. Both processes use the same subroutine to generate the range of MCA input levels and therefore the output data files can be directly related to each other.

3.5.4 Measurement Results

As mentioned in Chapter 1 three seperate MCA's are used for evaluation of the IM_3 prediction software. A practical IM_3 measurement must first be carried out for this purpose. The first MCA operates at 100 MHz with a 100 kHz channel spacing and has a gain of 19 dB and a P_1 dB compression point at 2 dBm. The second MCA was designed to operate within the DCS-1800 band, 1.71 GHz to 1.88 GHz, with a 200 kHz channel spacing and provides 10 dB of gain with a 1-dB compression point at 10 dBm. The third and final device is a MCPA designed to operate within the DECT band, 1.88 GHz to 1.9 GHz, with a 1 MHz spacing and provides in excess of 10 dB gain and has 1-dB compression at 11 dBm.

As a large number of measurements are carried out on each MCA an extract of the results will be presented here only. Table 3.1 displays an extract from the input data

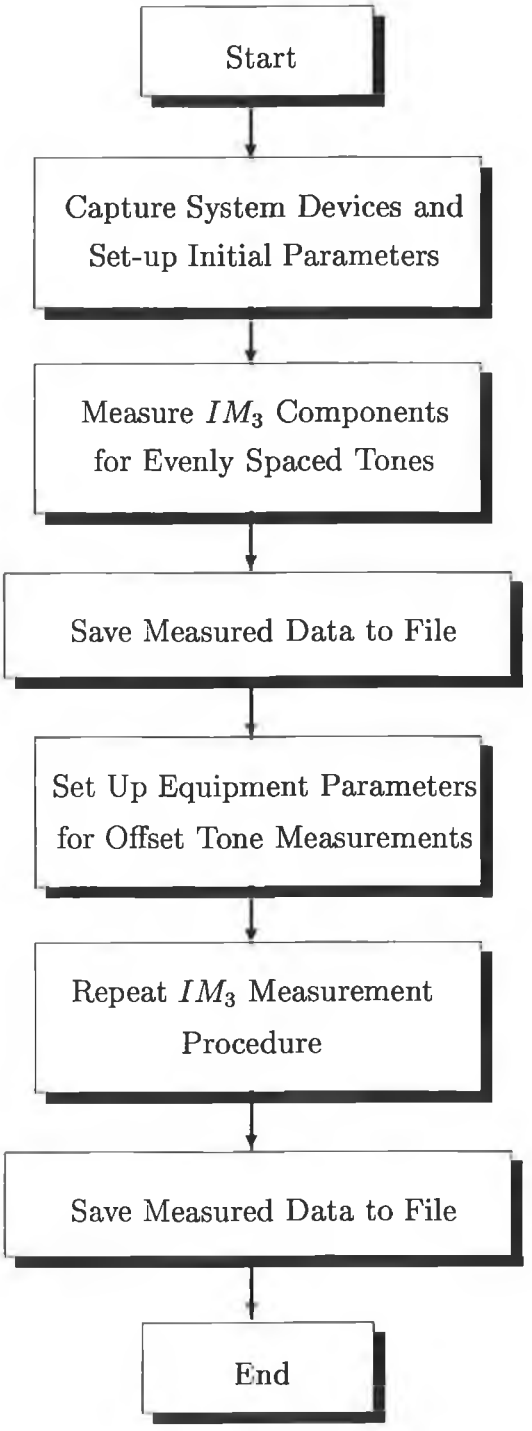

Figure 3.4: Measurement program flowchart.

file for the 100 MHz MCA. Table 3.2 shows the relating output data file for evenly spaced tones. Due to the large number of IM_3 products generated, the relating output data file for unevenly spaced tones is divided between Tables 3.3 and 3.4. All measurements are in dBm.

P_{f_1}	P_{f_2}	P_{f_3}
-30.00	-29.00	-28.00
-29.00	-28.00	-27.00
-28.00	-27.00	-26.00
-27.00	-26.00	-25.00
-26.00	-25.00	-24.00
-25.00	-24.00	-23.00
-24.00	-23.00	-22.00
-23.00	-22.00	-21.00

Table 3.1: Table showing an extract of the input data for the 100 MHz MCA.

$P_{2f_1-f_3}$	$P_{2f_1-f_2}$	P_{f_1}	P_{f_2}	P_{f_3}	$P_{2f_3-f_2}$	$P_{2f_3-f_1}$
-71.21	-63.37	-18.26	-17.16	-16.21	-62.19	-69.45
-68.83	-60.83	-17.41	-16.34	-15.29	-59.86	-66.97
-65.69	-57.68	-16.46	-15.17	-14.32	-56.24	-63.88
-62.88	-54.34	-15.53	-14.30	-13.17	-53.19	-60.67
-60.04	-51.78	-14.52	-13.24	-12.27	-50.18	-57.81
-57.06	-48.71	-13.67	-14.44	-11.36	-47.48	-55.01
-53.89	-45.47	-12.63	-11.36	-10.42	-44.24	-52.50
-50.98	-41.93	-11.51	-10.48	-9.48	-41.12	-49.25

Table 3.2: Table showing an extract of the corresponding output data for the 100 MHz MCA with evenly spaced tones.

$P_{2f_1-f_3}$	$P_{2f_1-f_2}$	$P_{f_2+f_1-f_3}$	$P_{2f_2-f_3}$	P_{f_1}	P_{f_2}	$P_{f_1+f_3-f_2}$
-72.17	-66.71	-73.64	-70.87	-18.31	-17.60	-66.36
-70.19	-64.45	-72.88	-67.27	-18.39	-16.60	-64.64
-68.10	-61.32	-69.70	-64.36	-17.45	-15.69	-61.37
-65.46	-58.44	-67.05	-61.70	-16.69	-14.58	-58.84
-62.19	-55.22	-64.10	-58.43	-15.59	-13.69	-55.52
-59.68	-52.48	-61.91	-55.67	-14.87	-12.80	-52.90
-76.83	-56.59	-49.46	-58.17	-13.51	-11.73	-52.67
-74.42	-53.60	-46.38	-55.35	-12.77	-10.87	-49.68

Table 3.3: Table showing an extract of the corresponding output data for the 100 MHz MCA with f_3 offset by 10 kHz.

$P_{2f_2-f_1}$	P_{f_3}	$P_{2f_3-f_2}$	$P_{f_2+f_3-f_1}$	$P_{2f_3-f_1}$
-72.39	-16.53	-66.63	-69.53	-70.65
-70.63	-15.38	-64.91	-66.50	-68.37
-68.49	-14.50	-61.88	-63.85	-66.54
-64.96	-13.33	-59.23	-60.29	-62.54
-62.76	-12.45	-56.05	-57.73	-59.48
-59.21	-11.51	-53.22	-54.57	-56.61
-49.99	-10.79	-56.03	-49.99	-52.13
-46.79	-9.71	-53.31	-47.18	-49.15

Table 3.4: Continuation of Table 3.3 showing an extract of the corresponding output data for the 100 MHz MCA with f_3 offset by 10 kHz.

Chapter 4

Analysis of Weakly Nonlinear Circuits

4.1 Introduction

"*In communication circuits the designer's ability to control phenomena such as nonlinear distortion is critical to the system's performance, so nonlinear circuit analysis is essential*", Steven Maas [24].

In Chapter 3 a measurement system was presented that accurately recorded IM_3 behaviour in MCA's. In this Chapter the Volterra-series approach to nonlinear circuit analysis will be introduced and developed into a form that can be used for predicting these IM_3 levels. As a number of other techniques have been successfully employed for nonlinear circuit analysis it is necessary to discuss these with a view to justifying the usage of the Volterra-series. In general, nonlinear analysis methods can be classified as being either time-domain, frequency-domain or hybrid (mixed time- and frequency-domain) depending upon the technique employed [25]. Volterra-series falls into the category of frequency-domain analysis. In the following section the two other methods, time-domain and hybrid, will first be discussed.

4.2 Time-Domain and Hybrid Methods

4.2.1 Time-Domain Method

Time-domain methods generally rely on numerical integration or, where possible, calculate the instantaneous value of the output (e.g. current) of a circuit element from the instantaneous value of the input (e.g. voltage) to it. An example of the time-domain approach is the popular SPICE[1] program. Time-domain methods generally suffer from two major inconveniences which halt its contention as a method for IM_3 prediction in MCA's. The first being its inability to deal effectively with complex distributed circuits such as the MCA's considered here. A solution must be obtained iteratively at each of many successive time intervals which for complex circuits can be a long process. Secondly, time-domain analysis would typically spend most of its computational effort on transient evaluation, while most of the user's interest is concentrated on steady-state information [24][26].

4.2.2 Harmonic-Balance Method

A hybrid technique for analysing RF nonlinear circuits is the Harmonic-balance method [27][28][29]. While this method is frequently classified as frequency-domain, it is more appropriately called a hybrid method since much of the analysis is explicitly done in the time-domain. This technique effectively partitions a RF circuit into two subcircuits: the linear subcircuit which contains all the linear parts, and the nonlinear subcircuit which contains only nonlinear elements. The linear elements are analysed in the frequency-domain and the nonlinear elements in the time-domain. The frequency- and time-domain quantities are usually related by the Fourier transform. Harmonic-balance, again, does not meet the prerequisites as a technique for IM_3 prediction in MCA's. It is inherently very slow, requiring a lot of computer memory and processing power. Secondly, the Fourier transform has limited numerical range and an inability to deal efficiently with multi-tone excitations [24]. This

[1]Simulation Program with Integrated Circuit Emphasis, Elec. Res. Lab., Univ. of California, Berkeley

technique is applicable primarily to strongly nonlinear circuits that are excited by a large signal source.

4.3 Volterra-Series Analysis

4.3.1 Background of the Volterra-Series

The Volterra-series approach to nonlinear analysis is a frequency-domain approach that predates both Harmonic-Balance and time-domain analysis. Despite this fact and the fact that it works well for precisely the types of problems where traditional approaches are poor (i.e. weakly nonlinear circuits under multi-tone excitation) the Volterra-series did not become a serious contender in RF circuit analysis until recent years. The Spanish mathematician Vito Volterra first introduced the notion of what is now known as a Volterra-series in the 1930's. His work was futher developed by Norbert Wiener at M.I.T. in the 1950's when he showed that the input/output relationship of certain nonlinear systems could be conveniently represented by means of the Volterra-series expansion. The first practical application of this work was made in 1967 by Narayanan [12] who used Volterra-series to predict intermodulation distortion in transistor amplifiers thus paving the way for future applications. In the following section an explanation of the Volterra-series and its associated terminology will be given. A discussion on the benefits of the Volterra-series and it's applicability to this project will be presented in Section 4.3.3. In Section 4.3.4, the Volterra-series will be further developed into a format more suitable for incorporation into an IM_3 prediction tool.

4.3.2 Volterra-Series Explained

This explanation of the Volterra-series will generally follow that given by Weiner and Spina [12] and Maas [16]. To begin, consider a linear, causal system with memory

which can be completely described by the convolution integral

$$y(t) = \int_{-\infty}^{\infty} h(\tau)\, x(t-\tau) d\tau \tag{4.1}$$

where $x(t)$ is the input, $y(t)$ is the output and $h(t)$ is the impulse response of the linear system. The impulse response is seen to be a complete characterisation of the linear circuit in the sense that knowledge of the impulse response is sufficient to enable determination of the circuit response to any input. Now, remember that the power series expansion in (2.10) describes a weakly nonlinear system without memory having second- and third-order nonlinearities only. A generalised description of a nonlinear system without memory can therefore be given by the Taylor series

$$y(t) = \sum_{n=1}^{\infty} a_n \left[x(t)\right]^n \tag{4.2}$$

where a_n are the Taylor series coefficients and n is the order of the nonlinearity. The conventional Volterra-series combines (4.1) and (4.2) to describe a nonlinear system with memory

$$\begin{aligned} y(t) \;=\; & \int_{-\infty}^{\infty} h_1(\tau_1)\, x(t-\tau_1) d\tau_1 \\ & + \int\int_{-\infty}^{\infty} h_2(\tau_1,\tau_2)\, x(t-\tau_1)\, x(t-\tau_2)\, d\tau_1\, d\tau_2 \\ & + \int\int\int_{-\infty}^{\infty} h_3(\tau_1,\tau_2,\tau_3)\, x(t-\tau_1)\, x(t-\tau_2) \\ & .\, x(t-\tau_3)\, d\tau_1\, d\tau_2\, d\tau_3 + \ldots \end{aligned} \tag{4.3}$$

In (4.3), τ_i is the time variable and $h_n(\tau_1, \tau_2, \ldots, \tau_n)$ is called the *nth-order Volterra kernel* or the *nth-order nonlinear impulse response.* For $n = 1$, observe that (4.3) is reduced to

$$y(t) = \int_{-\infty}^{\infty} h_1(\tau_1)\, x(t-\tau_1) d\tau_1 \tag{4.4}$$

which is the form of the response obtained in (4.1) for a linear circuit. Equation (4.3) can be expressed in the more compact form as the finite sum

$$y(t) = \sum_{n=1}^{N} y_n(t) \tag{4.5}$$

where

$$y_n(t) = \int\int \ldots \int_{-\infty}^{\infty} h_n(\tau_1, \tau_2, \ldots \tau_n)\, x(t-\tau_1)\, x(t-\tau_2) \ldots x(t-\tau_n)\, d\tau_1\, d\tau_2 \ldots d\tau_n \tag{4.6}$$

and terms above *Nth*-order have been omitted from the infinite series because they contribute negligibly to the output. The Volterra kernels, $h_n(\tau_1, \tau_2, \ldots, \tau_n)$, are determined solely by the weakly nonlinear circuit and are independent of the circuit excitation. This invariance of the Volterra kernels to circuit input is a highly desirable feature of the approach. The first N Volterra kernels completely characterise the weakly nonlinear circuit in the sense that knowledge of the Volterra kernels is sufficient to enable determination of the circuit response to any input.

Now, letting the input be the sum of Q sinusoidal signals, expressed as

$$x(t) = \sum_{q=1}^{Q} \mid E_q \mid \cos(2\pi f_q t + \theta_q) = \frac{1}{2} \sum_{q=-Q}^{Q} E_q \, exp(j2\pi f_q t) \tag{4.7}$$

and it is assumed that

$$E_{-q} = E_q^*, \; E_0 = 0, \; f_{-q} = -f_q \tag{4.8}$$

where the asterisk denotes the complex conjugate. Substituting (4.8) into (4.6); interchanging the order of summation and integration and rearranging the terms, $y_n(t)$ becomes

$$\begin{aligned} y_n(t) \;=\; & \frac{1}{2^n} \sum_{q_1=-Q}^{Q} \sum_{q_2=-Q}^{Q} \cdots \sum_{q_n=-Q}^{Q} E_{q_1} E_{q_2} \ldots E_{q_n} \\ & . exp[j2\pi(f_{q_1} + f_{q_2} + \ldots + f_{q_n})t] \int\int \cdots \int_{-\infty}^{\infty} h_n(\tau_1, \tau_2, \ldots \tau_n) \\ & . exp[-j2\pi(f_{q_1}\tau_1 + f_{q_2}\tau_2 + \ldots + f_{q_n}\tau_n)] \, d\tau_1 \, d\tau_2 \ldots d\tau_n \end{aligned} \tag{4.9}$$

The terms from the integral sign to the end of (4.9) can be recognised as a multi-dimensional Fourier transform:

$$\begin{aligned} H_n(f_{q_1}, f_{q_1}, \ldots, f_{q_n}) \;=\; & \int\int \cdots \int_{-\infty}^{\infty} h_n(\tau_1, \tau_2, \ldots \tau_n) \\ & . exp[-j2\pi(f_{q_1}\tau_1 + f_{q_2}\tau_2 + \ldots + f_{q_n}\tau_n)] \\ & . d\tau_1 \, d\tau_2 \ldots d\tau_n \end{aligned} \tag{4.10}$$

Consequently, the nth-order response (4.9) may be rewritten as

$$\begin{aligned} y_n(t) \;=\; & \frac{1}{2^n} \sum_{q_1=-Q}^{Q} \sum_{q_2=-Q}^{Q} \cdots \sum_{q_n=-Q}^{Q} E_{q_1} E_{q_2} \ldots E_{q_n} H_n(f_{q_1}, f_{q_2}, \ldots, f_{q_n}) \\ & . exp[j2\pi(f_{q_1} + f_{q_2} + \ldots + f_{q_n})t] \end{aligned} \tag{4.11}$$

observe that the first-order transfer function is given by

$$H_1(f_1) = \int_{-\infty}^{\infty} h_1(\tau_1)\, exp[-j2\pi f_{q_1}\tau_1]\, d\tau_1 \tag{4.12}$$

which is the Fourier transform of the impulse response of the linear portion of the circuit. Therefore, $H_1(f_1)$ is the frequency domain linear transfer function or Volterra kernel equivalent to $h_1(\tau_1)$ in the time domain. More generally, specification of the time-domain Volterra kernels, $h_n(\tau_1, \tau_2, \ldots, \tau_n)$, is equivalent to specification of the frequency-domain Volterra kernels or nonlinear-transfer-functions (NLTFs), $H_n(f_{q_1}, f_{q_2}, \ldots, f_{q_n})$. As revealed in (4.11), $H_n(f_{q_1}, f_{q_1}, \ldots, f_{q_n})$ is the nonlinear-transfer-function relating the output at frequency at $(f_{q_1} + f_{q_1}+, \ldots + f_{q_n})$ to the input at frequencies $f_{q_1}, f_{q_2}, \ldots, f_{q_n}$.

To avoid ambiguity, the term "Volterra kernel" will be used solely for time-domain specification and likewise the term "nonlinear-transfer-function" will be used solely for frequency-domain specification. Also, all NLTFs can be shown to be equivalent if they differ only by a permutation of their arguments and are, therefore, symmetrical functions of their arguments. For example, third-order NLTFs with inputs f_1, f_2 and f_3 satisfy the relations

$$H_3(f_1, f_2, f_3) = H_3(f_1, f_3, f_2) = H_3(f_2, f_3, f_1) = H_3(f_2, f_1, f_3) = H_3(f_3, f_2, f_1) \tag{4.13}$$

When the signs of all arguments are changed the conjugation property also holds:

$$H_n(-f_{q_1}, -f_{q_2}, \ldots, -f_{q_n}) = H_n^*(f_{q_1}, f_{q_2}, \ldots, f_{q_n}) \tag{4.14}$$

where, once again, the asterisk denotes the complex conjugate.

4.3.3 Applicability of the Volterra-series

Volterra-series in essence uses a recursive method for analysing weakly nonlinear circuits directly in the frequency-domain making it computationally more efficient (and therefore faster) than either Harmonic-balance or time-domain methods. Furthermore, no Fourier transforms are used, so the numerical range is limited only by machine precision [24]. It also transpires that the NLTFs can be extracted using

a number of different methods. Nonlinear circuit modeling techniques such as the Harmonic-Input method or the Nonlinear currents method may be used to derive the NLTFs [16]. Modelling generally proves to be expensive, time consuming and in some cases application specific. By exploiting the fact that Volterra-series allows for NLTF determination through practical measurement techniques, nonlinear circuit modelling can be avoided.

Since a prerequisite for the IM_3 prediction tool is that an MCA's nonlinearities can be characterised (i.e. the NLTFs can be obtained) without using circuit modelling, the Volterra-series is an attractive approach. Another attractive feature is that the Volterra-series can easily deal with multi-tone excitations of various amplitudes. Volterra-series accuracy does suffer if the excitation signals become too large as higher order terms begin to dominate. This, however, is not a problem as the amplifiers considered here are operating below saturation where third-order terms dominate.

4.3.4 Determination of the NLTFs

As stated in the previous section, the NLTFs have to be extracted using a practical measurement technique. In order to do this the Volterra-series must first be developed further. From Section 2.2.1 it is apparent that even for relatively few excitation tones, Q, and a small order of nonlinearity, n, a very large number of IMD components are generated. The problem is simplified by virtue of the fact that only the IM_3 components that fall close to the excitation tones need to be considered. This still leaves the problem of determining the manner by which these IM_3 components are generated as a number of IM_3 terms can combine (fall at the same frequency) to create a composite IM_3 component. Weiner and Spina [12] developed the frequency mix concept for exactly this purpose.

Consider a circuit with three excitation tones ($Q = 3$) and a third-order nonlinearity ($n = 3$). The excitation tones are given by f_1, f_2 and f_3 and are equally spaced thus creating a number of composite IM_3 components (can be visualised in Figure 2.2). The composite IM_3 product at $2f_3 - f_2$ is produced by the two frequency mixes:

(1) $(f_3 + f_3 - f_2)$ and (2) $(f_2 + f_3 - f_1)$. As far as frequency mixes are concerned, the order in which the frequencies appear is unimportant. Therefore, $(f_3 + f_3 - f_2)$ represents the same mix as $(f_3 - f_2 + f_3)$. A mix is characterised by the number of times the various frequencies are involved. $(f_3 + f_3 - f_2)$ involves $-f_2$ once and f_3 twice. Now, let the number of times that the frequency f_k appears be denoted by m_k. All possible frequency mixes are then presented by the frequency mix vector

$$\mathbf{m} = (m_{-Q}, \ldots, m_{-1}, m_1, \ldots, m_Q) \tag{4.15}$$

Therefore the frequency mix $(f_3 + f_3 - f_2)$ is represented by $\mathbf{m} = (0, 1, 0, 0, 0, 2)$. Similarly, $\mathbf{m} = (0, 0, 1, 0, 1, 1)$ represents $(f_2 + f_3 - f_1)$. The output frequencies in (4.11) can be interpreted as those IMD frequencies that can be generated by all possible choices of m_k's such that following equation is satisfied:

$$\sum_{\substack{k=-Q \\ k\neq 0}}^{Q} m_k = m_{-Q} + \ldots + m_1 + m_1 +, \ldots + m_Q = n \tag{4.16}$$

Given a particular vector $\mathbf{m}$, the number of different ways that n indices $q_1, \ldots, q_n$ can be partitioned such that $-Q$ appears $m_{-Q}, \ldots, -1$ appears m_{-1} times, 1 appears m_1 times, ..., and Q appears m_Q times is given by the multinomial coefficient

$$(n; \mathbf{m}) = \frac{(n!)}{(m_{-Q}!) \ldots (m_{-1}!)(m_1!) \ldots (m_Q!)} \tag{4.17}$$

Again, using the same example, $n = 3$ and $\mathbf{m} = (0, 1, 0, 0, 0, 2)$ for $(f_3 + f_3 - f_2)$; the number of terms contributing to the mix is found using (4.17) as follows

$$(3; 0, 1, 0, 0, 0, 2) = \frac{(3!)}{(0!)(1!)(0!)(0!)(0!)(2!)} = 3 \tag{4.18}$$

Now, recall that several different frequency mixes may contribute to a particular IMD frequency component, f_m. Therefore, to obtain the total response at f_m, it is necessary to add together each of the various contributions. In general, the total response at frequency f_m is denoted $y(t; f)$. This is best illustrated using the above example again where the output

$$y(t; 2f_3 - f_2) = y_3(t; 0, 1, 0, 0, 0, 2) + y_3(t; 0, 0, 1, 0, 1, 1) \tag{4.19}$$

An important factor in determining the total response accurately at a particular f_m is the phase relationship of the individual terms as they may combine at various angles

relative to each other. As a practical phase measurement system is not available the response will be determined using magnitude information only. Although this seems like an oversimplification of the problem it does prove to be a useful development. The various contributions will now have to be added in-phase, therefore, giving a quite useful worst case prediction of IMD levels [11][30].

The Volterra-series will now be developed a stage further to allow for magnitude only information. Typically, an IMD component (in the case of this thesis an IM_3 component) at the output of a weakly nonlinear circuit is described in terms of it's average power delivered to the load. Therefore, it is necessary to develop an expression for the average powers in the input signals that generate the frequency mix. Assuming both $x(t)$ and $y(t)$ to be voltages, it is apparent from (4.11) that the nth-order NLTF has the dimensions of $volts^{1-n}$. The magnitude of the sinusoidal response corresponding to the vector $\mathbf{m}$ is

$$\mid E_{\mathbf{m}} \mid = \frac{(n;\mathbf{m})}{2^{n-1}} \mid E_1 \mid^{(m_1+m_{-1})} \ldots \mid E_Q \mid^{(m_Q+m_{-Q})} \mid H_n(\mathbf{m}) \mid \tag{4.20}$$

The average power dissipated by this component in a load having conductance $G_L(f)$ is

$$\begin{aligned} P_L(f_m) &= \frac{1}{2} \mid E_M \mid^2 G_L(f_m) \\ &= \frac{(n;\mathbf{m})^2}{2^{2n-1}} [\mid E_1 \mid^2]^{(m_1+m_{-1})} \ldots [\mid E_Q \mid^2]^{(m_Q+m_{-Q})} \mid H_n(\mathbf{m}) \mid^2 \\ &\quad . G_L(f_m) \end{aligned} \tag{4.21}$$

All power values will have units of watts unless stated otherwise. Similarly, if the input conductance of the weakly nonlinear system is $G_S(f)$, the average power of the input tone at the frequency f_q is

$$P_S(f_q) = \frac{1}{2} \mid E_q \mid^2 G_S(f_q) \tag{4.22}$$

from which it follows that

$$\mid E_q \mid^2 = \frac{2P_S(f_q)}{G_S(f_q)} \tag{4.23}$$

Use of (4.23) in (4.21) with the aid of (4.16) results in

$$P_L(f_m) = [P_S(f_1)]^{(m_1+m_{-1})} \ldots [P_S(f_Q)]^{(m_Q+m_{-Q})} c(\mathbf{m}) \tag{4.24}$$

where

$$c(\mathbf{m}) = \frac{(\mathbf{n};\mathbf{m})^2}{2^{2n-1}} \frac{|\ \mathbf{H_n(m)}\ |^2 \mathbf{G_L(f_m)}}{[\mathbf{G_S(f_1)}]^{(m_1+m_{-1})} \ldots [\mathbf{G_S(f_Q)}]^{(m_1+m_{-1})}}. \tag{4.25}$$

and is referred to as the intermodulation multiplier and has the dimension of $watts^{1-n}$.

Although it may not be completely obvious (if obvious at all!), the Volterra-series has been developed into a format that can easily be incorporated into a software algorithm for IM_3 prediction purposes. By re-arranging (4.24) in terms of the input and corresponding output powers a value for $c(m)$ can be obtained. Using this value for $c(\mathbf{m})$ in (4.25) and, again, re-arranging, the NLTF magnitude, $|\ H_n(\mathbf{m})\ |$, can be evaluated. Finally, substituting $|\ H_n(\mathbf{m})\ |$ into (4.21) gives the corresponding IM_3 amplitude in volts. Equation (4.22) can then be used to convert the result into watts.

Chapter 5

Prediction Tool Development

5.1 Introduction

In Chapter 3 an IM_3 measurement system was developed for MCAs operating below saturation. In the previous chapter the Volterra-series approach was introduced and developed into a set of expressions applicable to IM_3 prediction in MCAs. Now, using these developments as a basis, a robust software tool for IM_3 prediction in MCAs will be developed. This novel approach relies on a black-box style characterisation of the MCA and, therefore, may be applied to any MCA operating below saturation (i.e. in a weakly nonlinear mode). Two sets of IM_3 measurements (involving three tones) are all that is required to completely characterise the IM_3 behaviour of the MCA. An IM_3 prediction can then be made for an arbitrary number of excitation tones of various amplitudes using the Volterra-series approach [31]. In the following section an explaination of the actual prediction process will be given. Section 5.5 will give a formal description of the complete software algorithm.

5.2 Measurement Data

As mentioned in the introductory section, the prediction tool is comprised of an initial characterisation process followed by a Volterra-series based prediction. An

important MCA feature supplies the link between these two stages of the prediction process and effectively allows for a complex IM_3 prediction to be made using such limited measurement information. Lu *et al* [32] discovered that if $\Delta f < f_{TH}$, the dispersion transition frequency, the device will exhibit low-frequency dispersion effects and the IM_3 value will be dependant on Δf. When $\Delta f > f_{TH}$, IM_3 becomes independant of Δf. The silicon BJT devices considered here experience such effects as is shown in Figures 5.1, 5.2 and 5.3. In Figure 5.1, IM_3 is constant from 1 MHz to 5 MHz and rises sharply for $\Delta f < 1$ MHz. This sharp rise indicates that f_{TH} is located just below 1 MHz for this device. In Figures 5.2 and 5.3, IM_3 is approximately constant from 10 kHz to 6 MHz. As no sharp rise occurs in this region f_{TH} must be located below 10 kHz in these devices. The slight variations here are attributed to the bias circuitry. For any MCA there will be a designated first and last channel which equates to the maximum frequency spacing ($\Delta f = f_Q - f_1$). Also, the adjacent channel frequency seperation equates to the minimum channel spacing ($\Delta f = f_Q - f_{Q-1}$) in the MCA.

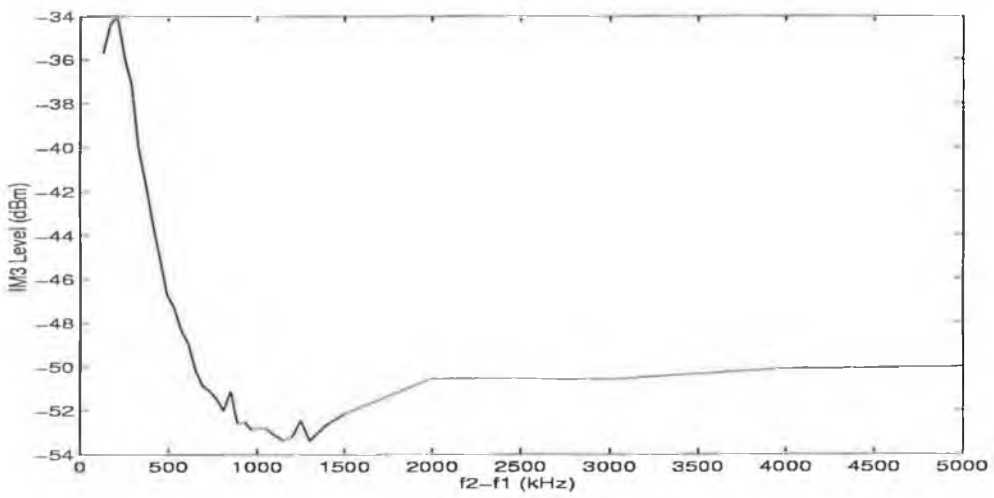

Figure 5.1: Measured IM_3 vs. Δf for MCA operating at 100 MHz with $f_1 = 100$ MHz and $P_{IN} = -20dBm$.

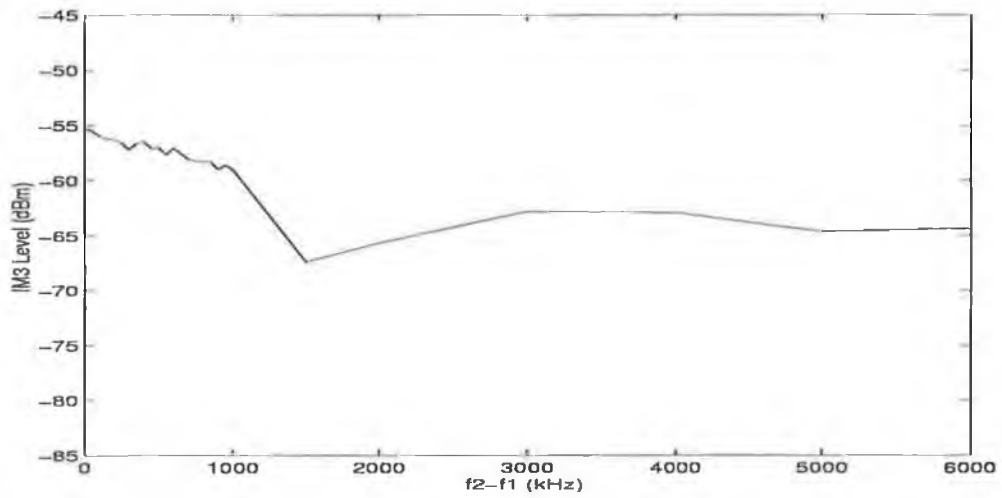

Figure 5.2: Measured IM_3 vs. Δf for MCA operating at 1800 MHz with $f_1 = 1800$ MHz and $P_{IN} = -22dBm$.

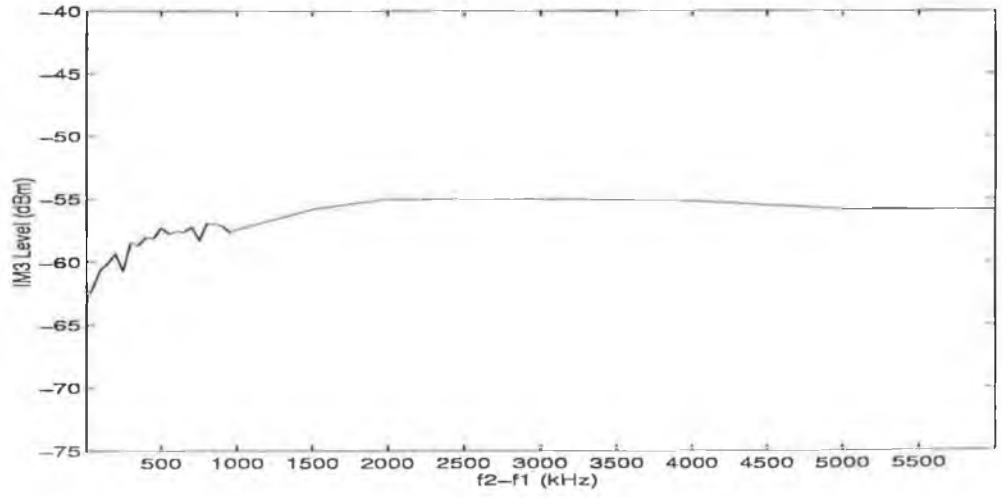

Figure 5.3: Measured IM_3 vs. Δf for MCA operating at 1880 MHz with $f_1 = 1880$ MHz and $P_{IN} = -12dBm$.

Now, two sets of IM_3 measurements (with one tone slightly offset in frequency as decribed in Section 3.2) are carried out; one for minimum Δf and one for maximum Δf. As before, the IM_3 components are of two types: those generated from two-tone IMD (see equation 3.2) and those generated from three-tone IMD (see equation 3.3). As a typical MCA will have a constant gain across it's required frequency range and the input measurement tones are of equal amplitude, the components $2f_1 - f_2$ and $2f_2 - f_3$ will have the same level as will $2f_2 - f_1$ and $2f_3 - f_2$ (see Figure 3.1). Therefore, for amplifier characterisation purposes, it is only necessary to input these values once.

5.3 Simulation

These sets of measurements along with the source and load impedances (typically 50Ω) are the only characterisation of the amplifier required. This information along with Δf, total number of channels, Q, individual channel frequencies and their corresponding power levels serve as the only inputs to the software program. Employing linear interpolation on each set of measured minimum and maximum frequency seperation data enables a power level to be generated for each frequency mix vector, $\mathbf{m}$, of interest. Before the corresponding NLTF magnitude, $\mid H_n(\mathbf{m}) \mid$, can be evaluated a value for $c(\mathbf{m})$ must be found by re-arranging (4.24) as follows

$$c(\mathbf{m}) = \frac{\mathbf{P_L(f_m)}}{[\mathbf{P_S(f_1)}]^{(\mathbf{m_1+m_{-1}})} \ldots [\mathbf{P_S(f_Q)}]^{(\mathbf{m_Q+m_{-Q}})}} \tag{5.1}$$

where $P_S(f_1) \ldots P_S(f_Q)$ are the input power levels for the measurement process and $P_L(f_m)$ is the interpolated power level relating to the IM_3 frequency of interest. Note, as the measurement process uses three equal amplitude tones, Q always equals three in equation (5.1). Also, note that Q is used to define the arbitrary number of MCA input tones in the prediction software as well.

Now, the corresponding NLTF is found by re-arranging (4.25) as follows

$$\mid H_n(\mathbf{m}) \mid = \sqrt{\frac{\mathbf{2^{2n-1}}}{\mathbf{(n;m)^2}} \frac{[\mathbf{G_S(f_1)}]^{(\mathbf{m_1+m_{-1}})} \ldots [\mathbf{G_S(f_Q)}]^{(\mathbf{m_1+m_{-1}})}}{\mathbf{G_L(f_m)}}} \tag{5.2}$$

If both the source and load impedances are equal to 50Ω the corresponding conductance is, therefore, equal to 0.02 *siemens*. This will greatly simplfy (5.2) as will be shown in Example 5.4. The predicted IM_3 amplitude, in volts, is given directly by (4.20) and can be converted into it's associated average power value (in watts) using (4.22).

A similar approach is used to obtain a predicted IM_3 power level for each of the frequency mix vectors. The individual IM_3 components that contribute to a composite IM_3 product are then added together in-phase. Finally, the IM_3 products are added to the the first-order (linear) response giving the complete output spectrum.

5.4 Example

To illustrate the above description of the prediction process, consider a MCA operating well below 1-dB compression within the DCS-1800 band which has a $\Delta f = 200\ kHz$. Both the source and load impedances are equal to 50 Ω. Let the input consist of three evenly spaced tones f_1, f_2 and f_3 with frequencies 1800.0 MHz, 1800.2 MHz and 1800.4 MHz respectively. The tones are arbitrarily assigned amplitudes of -10 dBm, -14 dBm and -12 dBm respectively. Note, as there are only three tones and a three tone measurement system is available this prediction procedure would not be required in reality. However, the purpose of this example is to display the prediction methodology in a non-complex manner.

To illustrate the behaviour at a composite IM_3 product consider the component at $2f_3 - f_2 = 1800.6\ MHz$ which is produced by two frequency mixes: (1) $(f_3 + f_3 - f_2)$ and (2) $(f_2 + f_3 - f_1)$. Assume that a measurement based characterisation has taken place with three equal amplitude excitation tones of -15 dBm and the corresponding power level for (1) is -63 dBm and for (2) is -56 dBm. The first step is to convert the input tones and (normally interpolated) frequency mix power levels from dBs to watts using

$$P(f)_W = log^{-1}\left[P(f)_{dB}/10\right] \tag{5.3}$$

and to convert the input power levels from dBs to volts using

$$| E_q | = log^{-1} [P_S(f_q)_{dB}/20]. \tag{5.4}$$

The frequency mix $(f_3 + f_3 - f_2)$, labeled (1), is represented by the frequency mix vector $\mathbf{m} = (0, 1, 0, 0, 0, 2)$. Similarly, $\mathbf{m} = (0, 0, 1, 0, 1, 1)$ represents $(f_2 + f_3 - f_1)$, labeled (2). The intermodulation multiplier, $c(\mathbf{m})$, can then be evaluated for (1) as follows:

$$\begin{aligned} c(\mathbf{m}) &= \frac{P_L(f_m)}{[P_S(f_1)]^{(m_1+m_{-1})}[P_S(f_2)]^{(m_2+m_{-2})}[P_S(f_3)]^{(m_3+m_{-3})}} \\ &= \frac{501.187 \times 10^{-9}}{[31.623 \times 10^{-3}]^3} = 15.849 \times 10^{-3}\ mWatts^{-2} \end{aligned} \tag{5.5}$$

and for (2)

$$\begin{aligned} c(\mathbf{m}) &= \frac{P_L(f_m)}{[P_S(f_1)]^{(m_1+m_{-1})}[P_S(f_2)]^{(m_2+m_{-2})}[P_S(f_3)]^{(m_3+m_{-3})}} \\ &= \frac{2.512 \times 10^{-6}}{[31.623 \times 10^{-3}]^3} = 79.435 \times 10^{-3}\ mWatts^{-2} \end{aligned} \tag{5.6}$$

The corresponding NLTF magnitudes can now be evaluated using (5.2) where the order of the nonlinearity, $n = 3$ and the source and load conductances are 0.02 Siemens. Again, starting with (1)

$$| H_3(0, 1, 0, 0, 0, 2) | = \sqrt{\frac{2^5}{3^2} \frac{0.02^3}{0.02} 15.849 \times 10^{-3}} \tag{5.7}$$

$$= \sqrt{22.541 \times 10^{-6}} = 4.748 \times 10^{-3} \tag{5.8}$$

And for (2)

$$| H_3(0, 1, 0, 0, 1, 1) | = \sqrt{\frac{2^5}{6^2} \frac{0.02^3}{0.02} 79.435 \times 10^{-3}} \tag{5.9}$$

$$= \sqrt{282.436 \times 10^{-6}} = 16.806 \times 10^{-3} \tag{5.10}$$

The predicted IM_3 amplitudes, in volts, are then given by 4.20. For (1)

$$\begin{aligned} | E_{(0,1,0,0,0,2)} | &= \frac{3}{4} . [199.526 \times 10^{-3}] . [251.189 \times 10^{-3}]^2 . 4.748 \times 10^{-3} \\ &= 44.830 \times 10^{-6}\ volts. \end{aligned} \tag{5.11}$$

Converting from *volts* to *watts* using (4.21) gives

$$P_L(f_{(0,1,0,0,0,2)}) = \frac{1}{2}.[44.830.10^{-6}]^2.0.02 = 20.098\,x\,10^{-12}\ watts \quad (5.12)$$

And converting to dBs

$$P_L(f_{(0,1,0,0,0,2)})_{dB} = 10log(P_L(f_{(0,1,0,0,0,2)}) = -106.969\ dBw. \quad (5.13)$$

Similarly for (2)

$$\begin{aligned} |\,E_{(0,1,0,0,1,1)}\,| &= \frac{3}{2}.[316.228\,x\,10^{-3}].[199.526\,x\,10^{-3}]^2.[251.189\,x\,10^{-3}]^2.4.748\,x\,10^{-3} \\ &= 23.773\,x\,10^{-3}\ volts. \end{aligned} \quad (5.14)$$

Converting from volts to watts:

$$P_L(f_{(0,1,0,0,1,1)}) = \frac{1}{2}.[23.773\,x\,10^{-3}]^2.0.02 = 5.652\,x\,10^{-6}\ watts \quad (5.15)$$

And converting to dBs

$$P_L(f_{(0,1,0,0,0,2)})_{dB} = 10log(P_L(f_{(0,1,0,0,1,1)}) = -52.478\ dBm. \quad (5.16)$$

To obtain the total response at 1800.6 MHz it is necessary to add together the individual contributions. From (4.19), the composite IM_3 product is given by

$$\begin{aligned} |\,E_{TOTAL}\,| &= |\,E_{(0,1,0,0,0,2)}\,| + |\,E_{(0,1,0,0,1,1)}\,| \\ &= 44.830\,x\,10^{-6} + 23.773\,x\,10^{-3}\ volts. \end{aligned} \quad (5.17)$$

Or in dBs

$$P_{TOTAL}(f_{IM}) = -52.462\ dBm. \quad (5.18)$$

This value is the predicted IM_3 power level at 1800.6 MHz. It is therefore a worst case prediction as it is assured that the composite tones are in phase. Under high drive levels or non resistive terminations this is rarely the case.

5.5 Software Description

The software program, written in Turbo C [23], which implements the entire prediction process will be described here. Figure 5.4 displays a flowchart of the overall

program operation. The program is sectioned into routines and subroutines which are called at various stages upon execution.

The INPUT function is first called by the program and the user is prompted for the required MCA information. The measured characterisation data must first be inputted, then the total number of channels, Q, the channel spacing, Δf, the source and load impedances and, finally, the individual channel frequencies and power levels. The CONVERT function is then called by the program. As described in Example 5.4, the inputted power values (in dBs) must be converted into units of watts and volts as required by the prediction process. Next, the PREDICTION function is called. As it's name suggets, this routines carries out the prediction and, therefore, incorpoates the linear interpolation and Volterra-series techniques.

As a large number of IM_3 components are generated when $Q \geq 3$, multi-dimensional arrays are used to ensure that each frequency component can be related to it's corresponding amplitude value. The first-order response is evaluated initially by adding the linear gain of the MCA to each of the input tones' amplitudes. Note, the first-order response will later be added to the third-order response so these fundamental tone amplitudes may change. Next, the IM_3 components generated from two-tone IMD are evaluated. Linear interpolation is employed on the measured data to predict a corresponding frequency mix power level. Volterra-series is then used, as in Example 5.4, to predict the corresponding IM_3 amplitude. Following this, the IM_3 components generated from three-tone IMD are dealt with in a similar manner.

The SORT routine then uses the "quicksort" algorithm [23] to sort the predicted IM_3 components in ascending order of frequency. All components falling at the same frequency are then added together and, finally, the IM_3 components are added to the first-order response to give the complete output spectrum. To verify and demonstrate the capability of this technique, predicted and measured results will be compared in the next chapter.

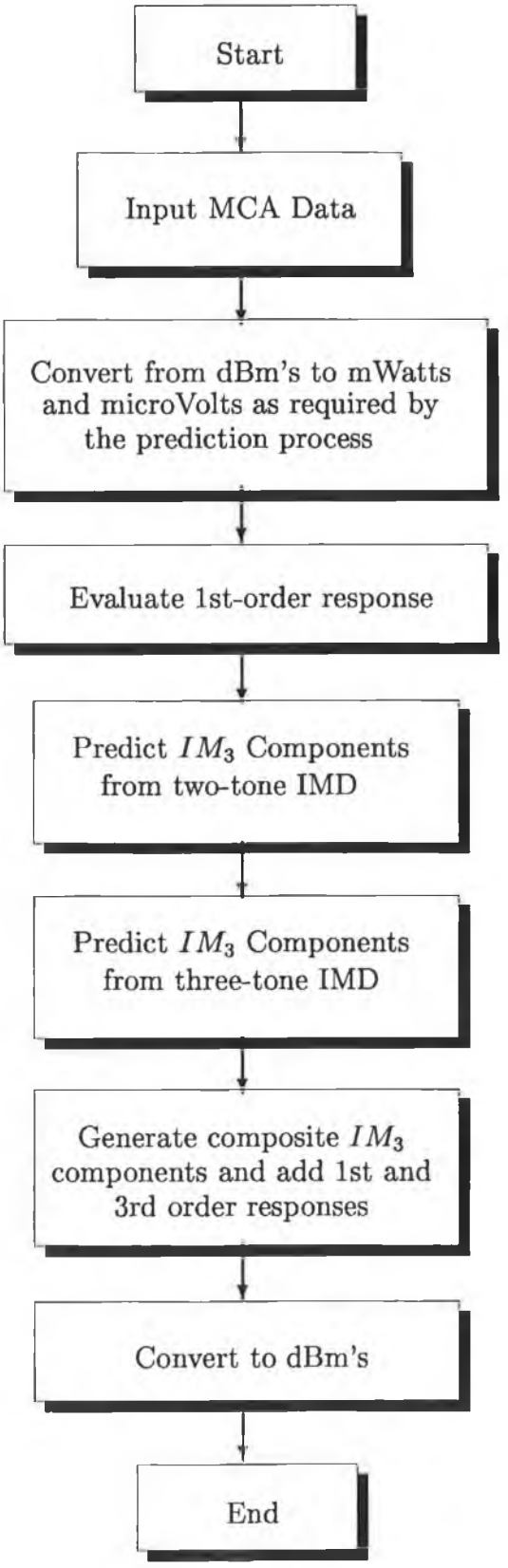

Figure 5.4: IM_3 prediction program flowchart.

Chapter 6

Prediction Tool Evaluation

6.1 Performance Evaluation Overview

To evaluate the performance of the prediction software a comparison is made between measured and predicted results for the MCAs decribed in the previous chapters. Initially, a comparison is made using a three-tone input and the measured results from Chapter 3. The channels are equally spaced and assigned different power levels. This will evaluate the software's ability to predict IM_3 levels for input tones of unequal amplitude. To further evaluate the prediction tool performance a fourth channel is introduced. The four channels are again assigned unequal amplitudes but are also unequally spaced in frequency. This comparison will evaluate the accuracy of using a linear interpolation technique to predict power levels for the individual frequency mixes. Following this, a comparison is made between predicted and measured results for two similar type 100 MHz MCAs in cascade. This further displays the capabilities of the software as IM_3 predictions are possible for cascaded stages.

6.2 Three-Tone Results

Figure 6.1 displays the results for the 100 MHz MCA with $\Delta f = 100$ kHz and the first tone is at 100 MHz. The corresponding input power levels are -32, -40 and -30 dBm respectively. Figures 6.2 and 6.3 show similar results for the other MCAs operating at 1800 MHz and 1880 MHz respectively. For the 1800 MHz MCA Δf is 200 KHz and the input powers are -19, -26 and -22 dBm respectively. The 1880 MHz device is a MCA with a Δf of 100 KHz and input powers of -13.39, -7.12, and -9.88 dBm respectively.

These results show the ability of the approach to simulate the amplifier's response to multiple tones with different power levels from a measurement using equi-power tones. Figures 6.1 and 6.3 show good agreement between predicted and measured IM_3 levels. Figure 6.2 shows some error but as the prediction is worst case and the prediction level is greater than the measured level the results are still valid.

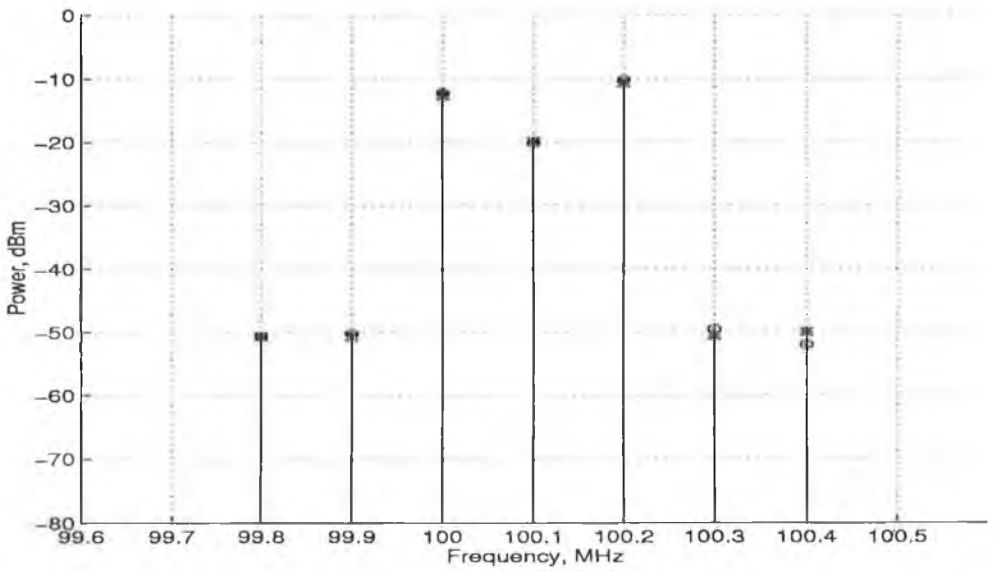

Figure 6.1: Measured vs predicted results for a 100 MHz MCA with a 3-tone input. Circles: Predicted values; Asterisk: Measured values.

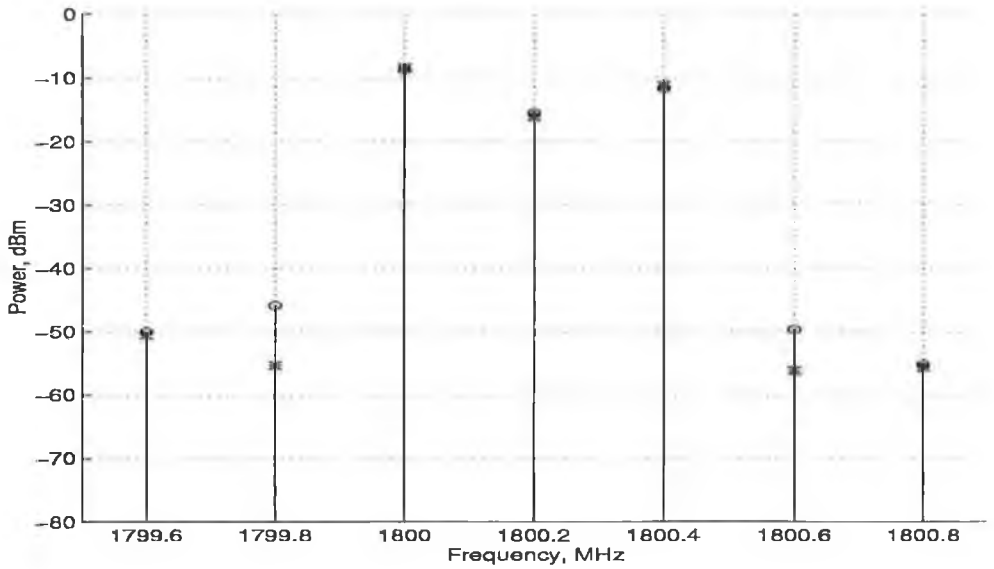

Figure 6.2: Measured vs predicted results for 1800 MHz MCA with a 3-tone input. Circles: Predicted values; Asterisk: Measured values.

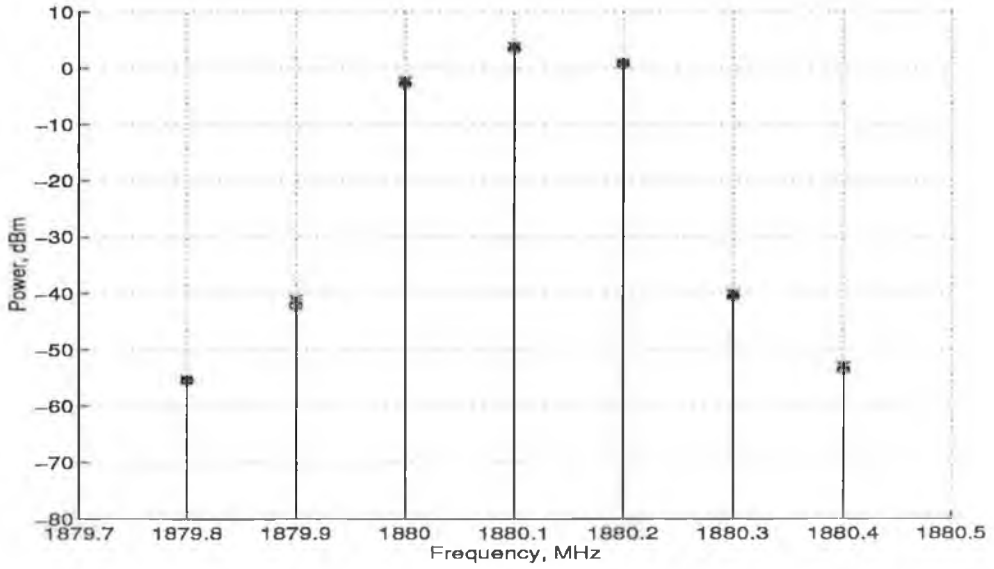

Figure 6.3: Measured vs predicted results for 1880 MHz MCA with a 3-tone input. Circles: Predicted values; Asterisk: Measured values.

6.3 Four-Tone Results

To further validate the new prediction tool, four tone excitations were used. Figure 6.4 gives the measured versus predicted results for the MCA operating at 100 MHz. The minimum Δf is 100 KHz and the maximum Δf is 500 KHz. Figure 5.1 clearly shows that the IM_3 level is dependent on Δf for this range of values. Figures 6.5 and 6.6 show similar results for the 1800 and 1880 MHz MCAs except that for their range the IM_3 level is independent of Δf (see Figures 5.2 and 5.3) and is approximately constant. These four-tone results display the ability of the IM_3 prediction tool to extrapolate from three tone measurement to four tone prediction. Again, the results are good with predicted levels generally greater than measurement and maximum errors of the order of 20 dB.

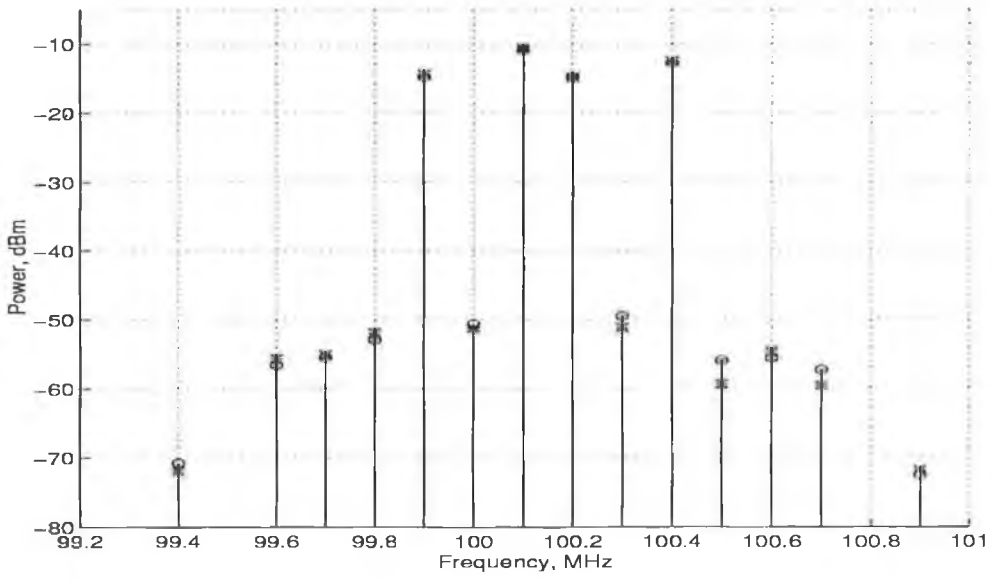

Figure 6.4: Measured vs predicted results for 100 MHz MCA with a 4-tone input. Circles: Predicted values; Asterisk: Measured values.

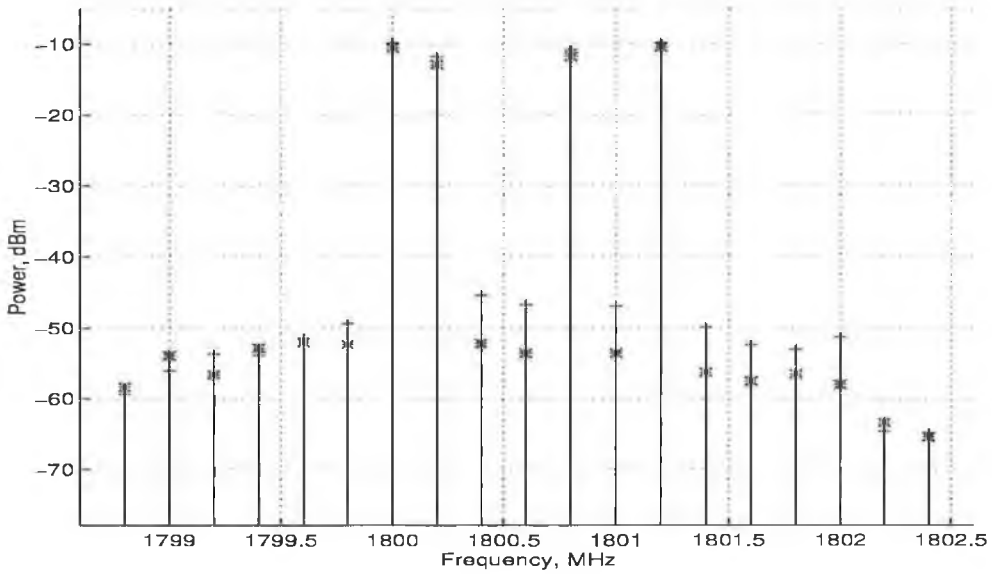

Figure 6.5: Measured vs predicted results for 1800 MHz MCA with a 4-tone input. Plus signs: Predicted values; Asterisk: Measured values.

6.4 Two-Stage MCA Results

To further illustrate the capabilities of the software an IM_3 prediction is made for two similar type MCAs in cascade. The technique for obtaining the IM_3 characteristics of cascaded stages is similar to that of single stages. The entire assembly can be treated as a black box system and a measurement based characterisation can be carried out as described in Chapter 6. Cripps [11] and Maas [30] state that a worst case assumption can still be used and the IM_3 components can be added in-phase. Cripps validates in-phase addition, stating that "*there is much more than a Murphy's Law chance of the worst happening, due to the inherent phase linearity of the system; the distortion products maintain their relative phases as they travel through the system in the same way that a pulse maintains it's shape as it travels along a dispersion-free transmission line*".

Figure 6.7 displays the result for two similar type 100 MHz MCAs in cascade where

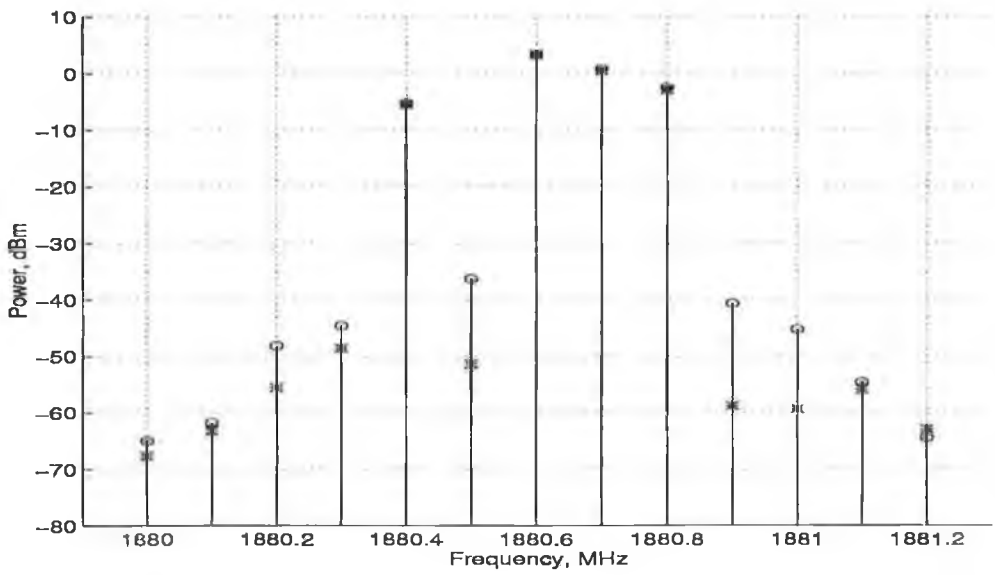

Figure 6.6: Measured vs predicted results for 1880 MHz MCA with a 4-tone input. Circles: Predicted values; Asterisk: Measured values.

maximum errors are of the order of 10 dB. This is a very significant result because the input to the second stage comprises of both low level IM_3 products and high level fundamental tones from the first stage, which makes the overall prediction much more complicated.

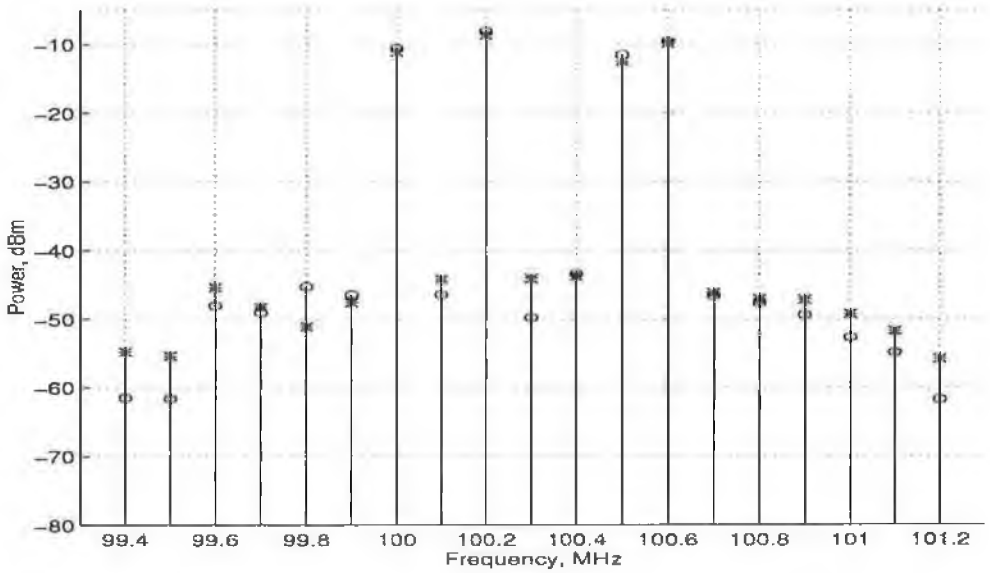

Figure 6.7: Measured vs predicted results for two 100 MHz MCAs in cascade with a 4-tone input. Circles: Predicted values; Asterisk: Measured values.

Chapter 7

MCPA Design

7.1 Introduction

In an increasing number of microwave multicarrier applications there is a need for MCPAs capable of delivering highly linear output levels with a high efficiency. Such MCPAs are currently in use as transmitter amplifiers in cellular base stations, satellite systems and digital television (DTV) systems. They will also be employed in future multicarrier applications such as third generation wideband CDMA cellular sytems [33], Microwave Video Distribution Systems (MVDS) [34] and broadband Asynchronous Transfer Mode (ATM) systems. The required specification is significantly different for satellite than for terrestrial applications. Satellite systems require a highly power efficient amplifier with a reasonable degree of linearity, which must be maintained over a broad bandwidth. In terrestrial land mobile applications, the "near-far" effect means that highly linear amplifiers are required to reduce the adjacent channel interference, and this necessitates a sacrifice of amplifier efficiency. In this application, linearity is the primary concern although it is also important for the overall system to be as power efficient as possible, thus reducing the size of the power supplies and cooling equipment and, hence, the cost of the equipment [35].

The two main characteristics of the amplifier which must, therefore, be considered are the linearity and DC to RF conversion efficiency. As these are generally condrat-

ictory, the MCPA design usually requires a compromise for a particular application. Both of these parameters have already been defined in Section 2.2 and 2.3 respectively. Traditionally, the IM_3 level was reduced by backing off the output power of the PA but this in turn reduces the efficiency [36]. In the remainder of this thesis a novel amplifier configuration that simultaneously improves upon efficiency and linearity will be described. Before introducing this technique in Section 7.3, an overview of the most effective existing techniques will be given in the following section.

7.2 Existing Techniques

The following is a list of the most commonly used techniques to acheive a high degree of linearity and efficiency in power amplifiers :

- Linear saturated amplifier with bi-directional control (LSA-BC) [37]: a dynamic bias of the drain combined with envelope feedback on the gain.
- Linear amplifiers using nonlinear components (LINC) [37]: the QPSK modulated signal is converted into two constant amplitude, phase modulated signals that drive two saturated amplifiers. The output of the amplifiers are then combined to reproduce the QPSK signal.
- Cartesian feedback [37]: the output signal is demodulated and compared to the input baseband signal. The resulting predistorted signal is remodulated by the saturated amplifiers.
- Adaptive predistortion [37]: the baseband signal is predistorted by a digital signal processor (DSP), modulated and amplified by a saturated amplifier. The output is demodulated and processed by a DSP in order to correct for the amplifier nonlinearities.
- Feedforward [38]: a sample of the amplifier output IMD components are amplified, phase inverted and nullified at the ouput coupler.

- Kahn Envelope Elimination and Restoration technique [39]: implements a linear amplifer by combining RF and AF power amplifiers. A limiter is used to eliminate the envelope, producing a constant amplitude, phase-modulated carrier. The detected envelope is amplified and amplitude modulation of the final RF PA restores the envelope of the phase-modulated carrier, creating a replica of the input signal.

All of these methods, and several of their variations, have shown very good IMD suppression results but at the price of highly complex systems. Their efficiency and physical size are degraded by high-speed dc-to-dc converters, DSP circuits or auxillary RF amplifiers which do not contribute to the output power. A new approach using an active biasing scheme will now be introduced which offers a high degree of linearity and efficiency for a relatively simplistic circuit.

7.3 The Active Biasing Technique

To produce a high-efficiency linear amplifier the previously introduced class A MCPA operating within the DECT band, 1.88 GHz to 1.9 GHz, is used. The amplifier provides in excess of 10 dB gain with reasonable impedance matching and has an output of 10 dBm at P_1 dB. It has poor efficiency, less than 5 %, and marginal adjacent channel IMD levels at P_1 dB. For verification purposes the amplifier can be switched between its normal bias configuration, a simple collector feedback circuit, to the active bias scheme which is presented here. As the technique uses a scaled version of the extracted envelope of the multi-tone signal to actively bias the amplifier a brief overview of multi-tone signals and their phase coherency is required.

7.3.1 Multi-tone Signal Overview

In general a multi-tone signal will contain some form of modulation thus making its phase coherency unperiodic. In order to simulate accurately the absolute worst case multi-tone signal condition it is necessary to have the peak voltages which occur

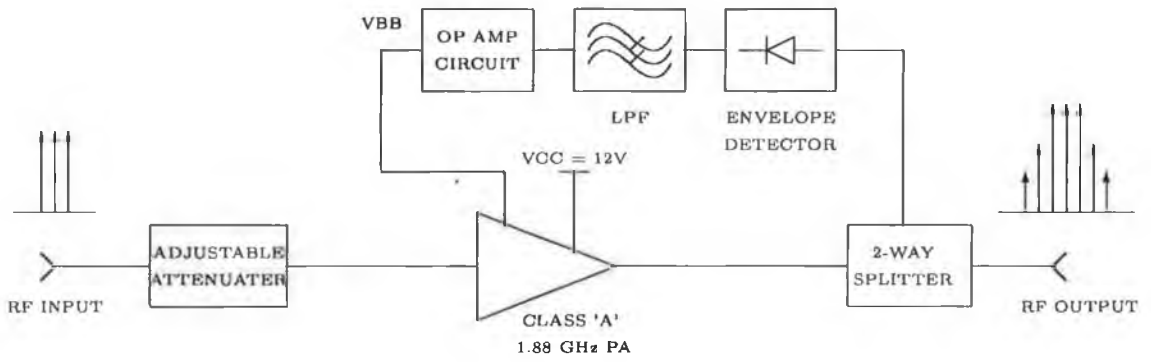

Figure 7.2: Block diagram of the active biased amplifier configuration.

envelope is extracted using a diode detector circuit based on a Schottky diode for a fast response time. Care must be taken to ensure that the time constant is long compared with the periodic time of the carrier wave and short compared with the periodic time of the envelope waveform [41]. The detector output is fed into a 3rd order Chebychev low-pass filter with a cut-off frequency of 100 MHz to supress the unwanted RF and its harmonic frequency components. The filtered detector output is then passed through a high speed non-inverting op amp with a variable feedback resistor to modulate the base current of the transistor. A block diagram of the amplifier configuration is shown in Figure 7.2.

Due to the low output level of the RF source the amplifier was constructed with a feedback configuration so that a sufficiently high voltage level could be supplied to the diode detector circuitry. With a sufficient input power level a feedforward active biasing technique would offer a greater improvement in both linearity and efficiency, η, as the envelope extracted from the RF output incorporates the distortion effects of the amplifier.

7.4 Low-Pass Filter Design

The low-pass filter design method used here takes advantage of normalised low-pass prototypes made available by Bowick [42]. The actual design procedure is, therefore, nothing more than determining the filter requirements and calculating the compo-

nent values using the corresponding prototype values. A cutoff frequency of 100 MHz is chosen so that the unwanted RF and associated harmonic frequency components are suppressed without placing a severe limit on the low frequency performance. The Chebychev response gives a steeper initial descent into the stopband and is, therefore, employed here. The low-pass prototype (showing element values) for the desired third-order Chebychev filter with a 0.01 dB ripple is given in Figure 7.3. The source and load resistances are both equal to 50 Ω.

To obtain the actual component values frequency and impedance scaling is used. The following formulas are used to carry out the transformation:

$$C = \frac{C_n}{2\pi f_c R} \tag{7.1}$$

$$L = \frac{RL_n}{2\pi f_c} \tag{7.2}$$

where C = the final capacitor value, L = the final inductor value, C_n = a low-pass prototype element value, L_n = a low-pass prototype element value, R = the final load resistance, f_c = the final cutoff frequency.

Using Equations (7.3) and (7.4) the component values are scaled as follows:

$$C_1 = \frac{1.181}{2\Pi(100X10^6)(50)} = 37\,pF$$

$$C_3 = \frac{1.181}{2\Pi(100X10^6)(50)} = 37\,pF$$

$$L_2 = \frac{1.821(50)}{2\Pi(100X10^6)} = 145\,nH$$

The closest realisable capacitor value was found to be 33 pF; an actual 0.145 uH inductor was used.

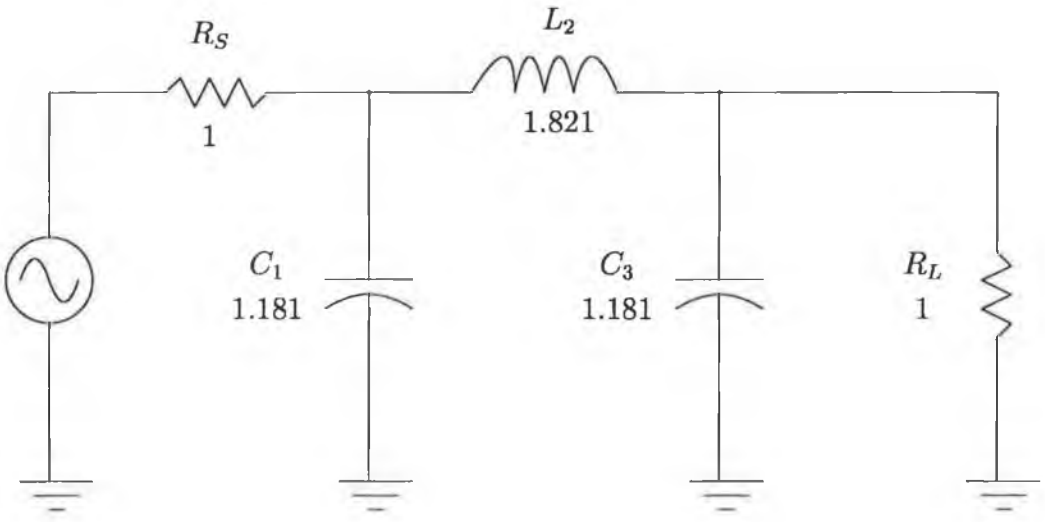

Figure 7.3: Chebychev low-pass prototype for 0.01 dB ripple.

Using a Wiltron 560 Scalar Network Analyser the measured transmission and reflection coefficient magnitudes are as in Figure 7.4. The plot displays a good impendance match for the LPF along with good supression.

7.5 Envelope Detector Design

The performance of the active biasing technique hinges largely on the ability to accurately measure the envelope of the multi-tone signal. The circuit has therefore been designed to have a fast response time and reasonable impedance matching within the DECT band. A Schottky diode BAT17 (D1) forms the basis of the detector design as is shown in Figure 7.5. The complete detector circuit consists of the diode in series with a parallel resistor-capacitor network, $R_2\,C_1$.

The time constant, τ , determines the rapidity with which the detected voltage can change, and must be long compared with the periodic time of the carrier wave and short compared with the periodic time of the envelope. The time constant for the charging of the capacitor is $r\,C_1$, where r is the forward resistance of the diode

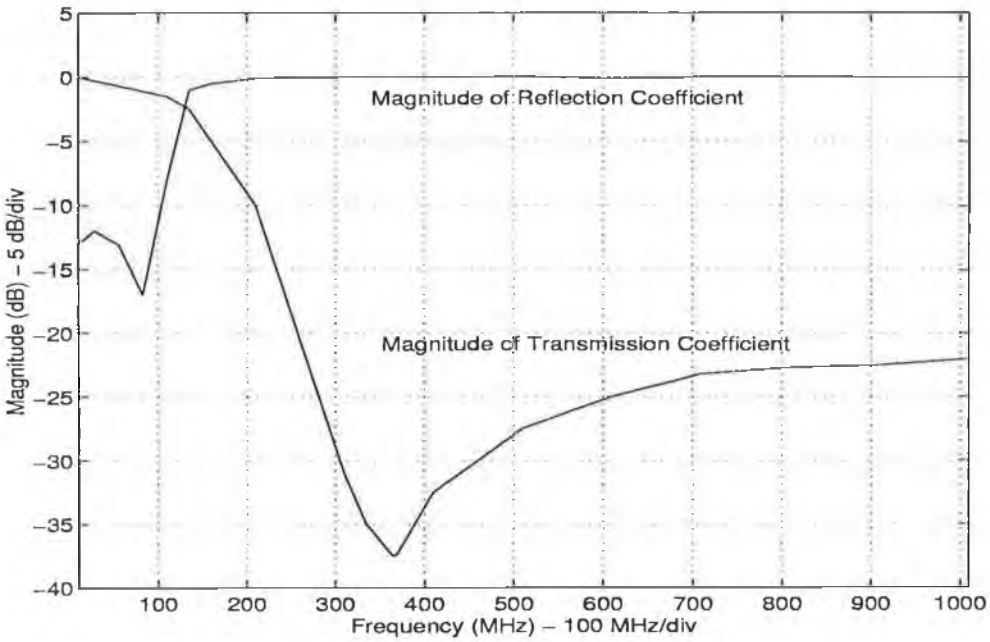

Figure 7.4: Plot of transmission and reflection coefficient magnitudes for the low-pass Chebychev filter with 0.01dB ripple.

estimated (from the data sheet) to be 10 Ω and C_1 equals 33 pF. This gives a value of 330 pico-seconds or a frequency of 3 GHz which implies that the detector should have no problem following the rising peak part of the modulation cycle for a carrier at approximately 1.9 GHz.

The time constant for the discharging of the capacitor is $R_2\ C_1$, where R_2 is the 1 $K\ \Omega$ load resistor, giving a value of 33 nano-seconds or a frequency of 30.3 MHz. This implies that Δf must be less than 30.3 MHz for accurate extraction of the envelope.

An important measurement to obtain is the diode detector characteristic which is a plot of the curve of detector output voltage versus detector input power. Figure 7.5 shows the detector characteristic with the input power varied using a 1 dB step attenuater until the output voltage drops below 100 mV. This plot identifies the linear region of operation for the detector and therefore the region in which it will operate most accurately.

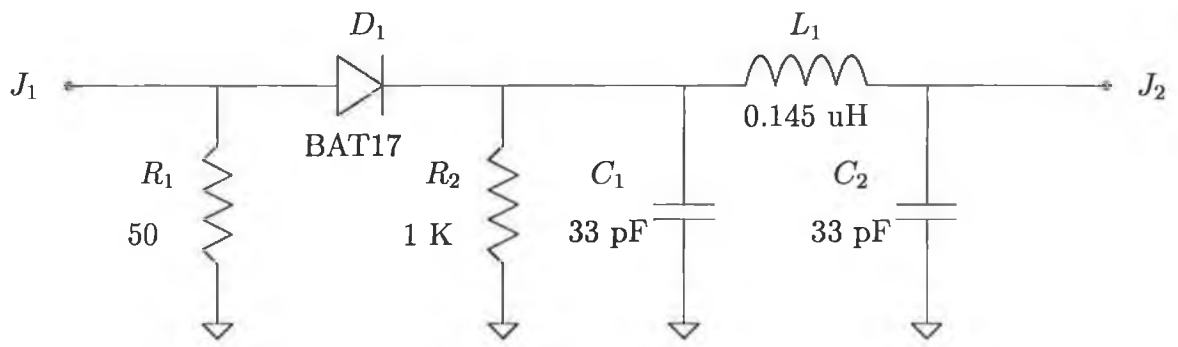

Figure 7.5: Envelope Detector and LPF Circuit Schematic.

7.6 Operational Amplifier Design

A high speed non-inverting operational amplifier with a variable feedback resistor is required to modulate the base current of the transistor. Figure 7.6 shows a schematic of the operational amplifier circuitry based on a LM6365 high speed operational amplifier. The operational amplifier should be chosen on the basis of slew rate which is dependant on the frequency of the modulating wave (equal to Δf), and on it's gain and noise capabilities. The slew rate is defined as the maximum rate of change of the operational amplifier's output voltage and in this case is 300 V/μS, which more than meets the requirements of the prototype circuit.

The series resistor-capacitor network between the operational amplifier's input pins (R_x , C_x) is added for noise-gain compensation at high frequencies. Their values are calculated using the following equations obtained from the operational amplifier data sheet:-

$$R_x\, C_x = \frac{1}{2}\pi\, 25\text{MHz} \tag{7.3}$$

$$[R_1 + R_F(1 + \frac{R_1}{R_2})] = 25\, R_x \tag{7.4}$$

After inputting the various component values R_x was evaluated to be 122 Ω and therefore C_x must be greater than or equal to 52 μF.

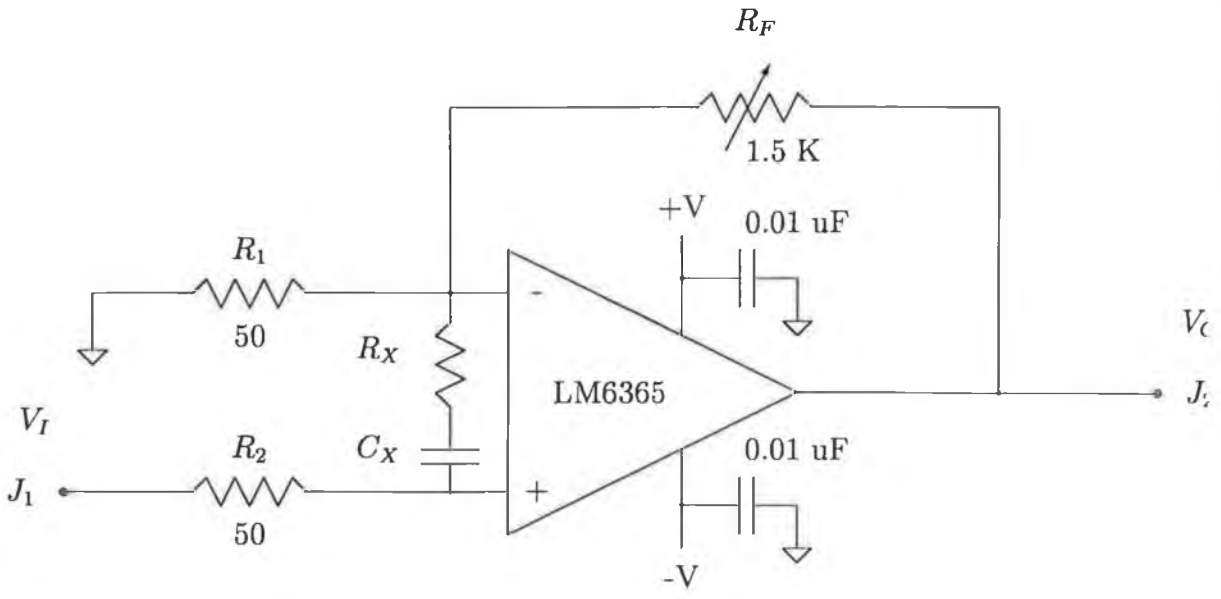

Figure 7.6: High Speed Operational Amplifier Circuit Schematic.

7.7 MCPA Performance

To demonstrate the performance of this circuit a comparison of worst case adjacent channel IMD levels and amplifier efficiency is made between the normal and active biased circuits. As stated previously, the normal bias circuit in this case is a simple collector feedback circuit and the multi-tone RF input is generated by three synthesised signal generators externally phase locked together.

Figures 7.7 and 7.8 show the results for the amplifier with a 50 kHz channel spacing. Operating just below P_1 dB, which occurs at an output of 10 dBm, the efficiency is improved from 2.4 % to 3.5 %. The highest adjacent channel IMD level, for the same output, is dramatically reduced from a value of -12dBc to -25dBc. Results for a 100 kHz channel spacing shown in Figures 7.9 and 7.10, also show an improvement in efficiency and linearity.

To further demonstrate the circuit's IMD performance a comparison is made between the active and normal biased circuit for all IMD components with a three tone even level input signal. Figures 7.11 and 7.12 display the IMD performance for normal and active biasing respectively.

These results display a distinct improvement in both efficiency and linearity. It is also very significant that these improvements have been achieved using a relatively simplistic circuit design. Other techniques have achieved similar results but at the expense of highly complex circuits.

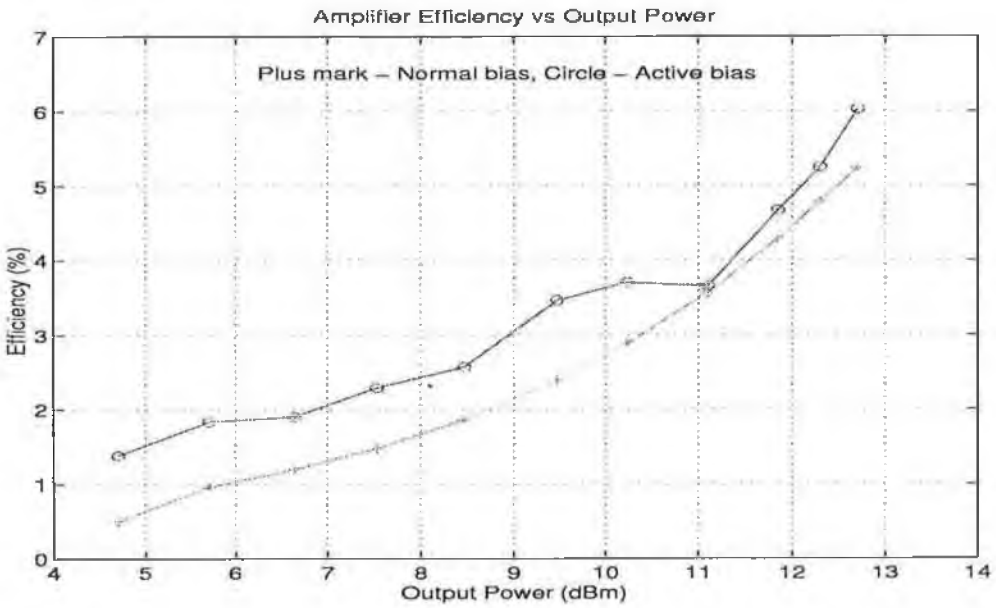

Figure 7.7: Efficiency versus output power for 50 KHz spacing.

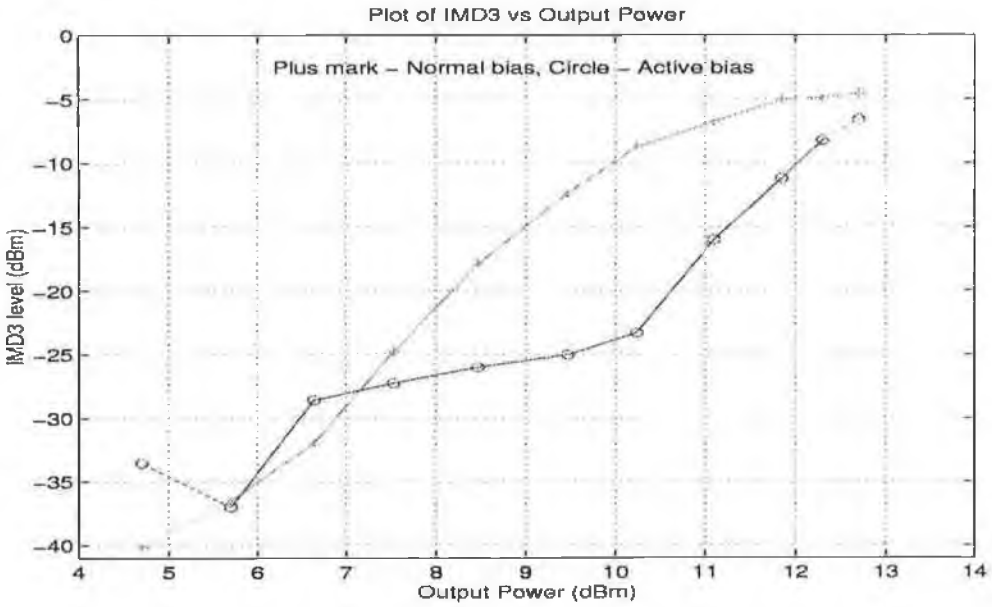

Figure 7.8: 3rd order IMD level versus ouput power for 50 KHz spacing.

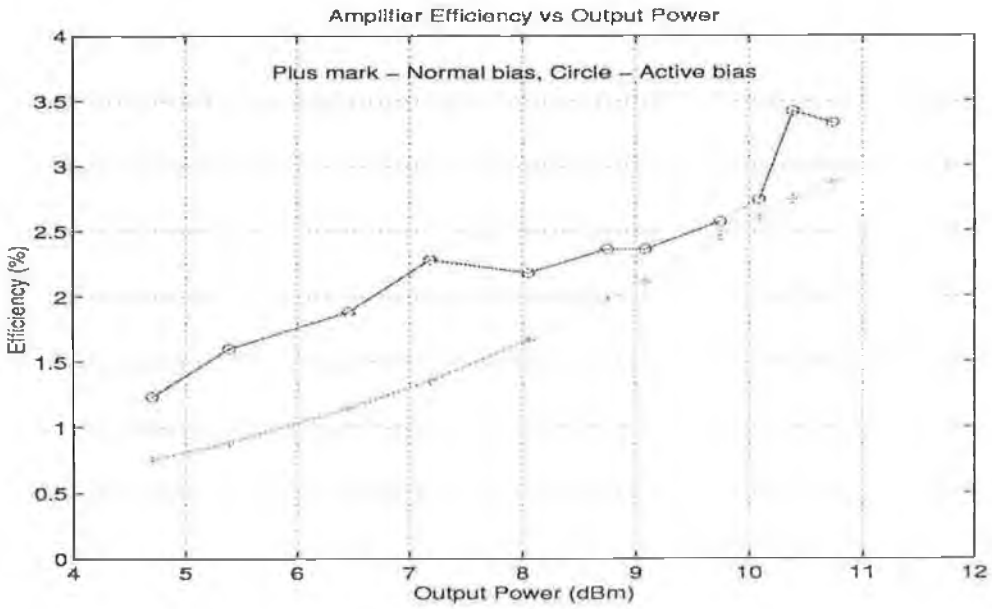

Figure 7.9: Efficiency versus output power for 100 KHz spacing.

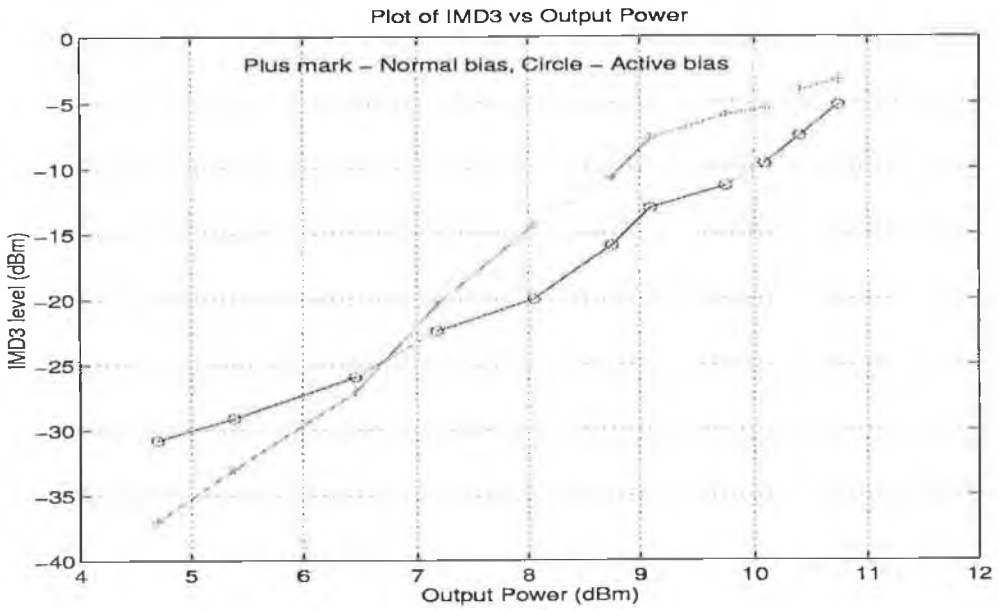

Figure 7.10: 3rd order IMD level versus ouput power for 100 KHz spacing.

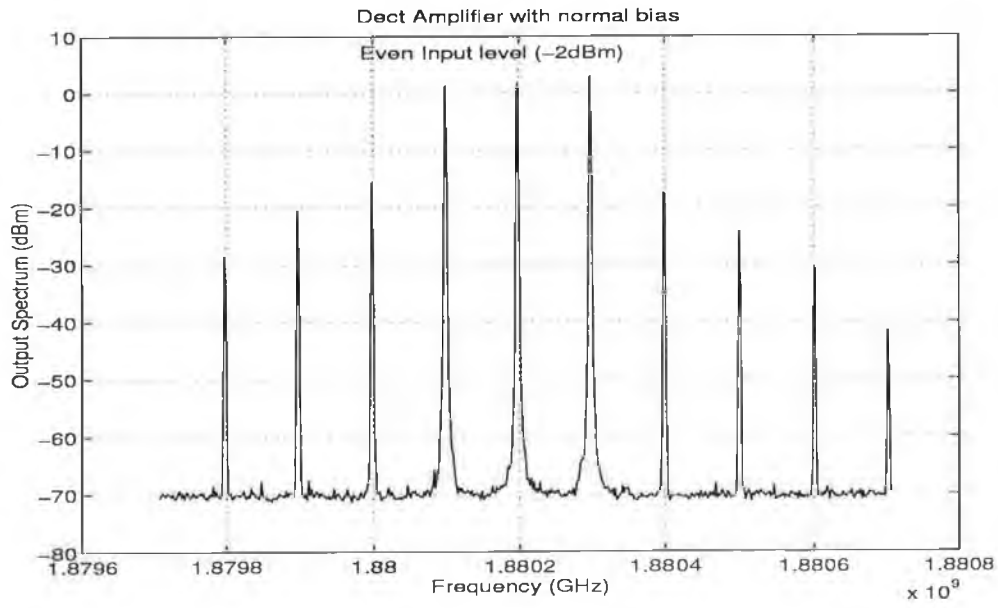

Figure 7.11: IMD levels for DECT MCPA with normal bias.

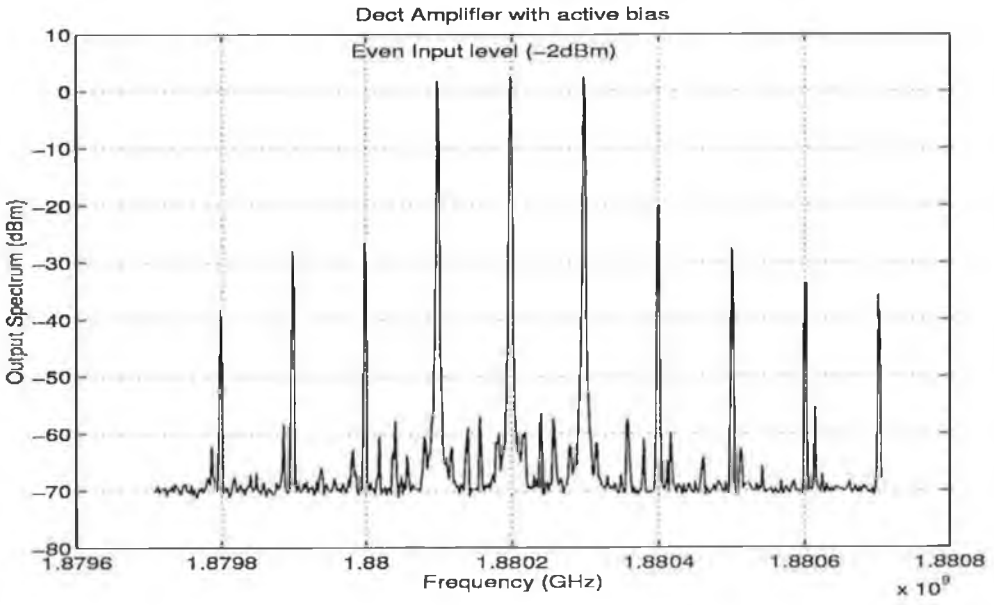

Figure 7.12: IMD levels for DECT MCPA with active bias.

Chapter 8

Conclusions and Future Recommendations

8.1 Introduction

This thesis addressed the issue of third-order intermodulation distortion (IM_3) in MCA's which are used in many modern wireless communication applications. The IM_3 problem has been investigated from two distinct viewpoints which is reflected in the structure of this thesis. The first section of this thesis has been devoted to the characterisation and prediction of IM_3 behaviour in MCA's without the use of complex circuit modelling. Following on from this, a novel amplifier configuration is presented which has been shown to reduce these IM_3 levels and simultaneously improve upon the overall amplifier efficiency. Future recommendations are set-out with regard to both sections, detailing areas for improvement and additional functionality which could be investigated.

8.2 IM_3 Prediction Tool

As the results of this thesis have shown, an IM_3 prediction tool has been sucessfully developed which can predict worst case IM_3 levels in MCA's. By exploiting the fact

that Volterra-series allows for the determination of the amplifier's nonlinear-transfer-functions (NLTFs) using practical measurement techniques, nonlinear circuit modelling has been avoided. This attractive feature of the Volterra-series greatly reduced the computational complexity of the prediction tool.

Another key factor in this approach was making use of the dependancy of IM_3 performance upon the frequency spacing of the carriers. This effectively allowed a complex prediction to be made using limited measurement information. Linear interpolation could then be employed to accurately estimate each of the frequency mix power levels. As only magnitude information had been available all individual frequency components that contribute to a composite IM_3 product were added together in-phase. This gave a quite useful worst case prediction of IM_3.

The results show the ability of the prediction tool to simulate an amplifier's response to multiple input tones with different power levels. A quite accurate prediction was also made for two similar type MCA's in cascade. This was a very significant result as the input to the second stage comprised of both low level IM_3 products and high level fundamental tones from the first stage making the overall prediction much more complicated. Maximum errors are in the order of 10 dB but as the prediction tool is for worst case IM_3 and the prediction level is greater than the measured level the results are still valid. It is felt that the technique owes it's accuracy to the close linkage between simulation and measurement and also to the use of three tome measurements instead of the more common two tone scenario.

A robust general purpose prediction tool has been developed which is of considerable use to RF System Designers. In reference to future development, it is felt that the accuracy of the tool could be further improved by obtaining a value for the dispersion transistion frequency through practical measurement. By using this information when applying linear interpolation a more accurate prediction of the frequency mix power levels could be made.

At a higher level, it appears that the prediction tool could be incorporated into a more general purpose RF system design tool where IM_3 predictions could be performed for multiple components in a circuit. A good example of this would be

base station transceiver design where predictions could be made on a per component basis with the ouput of the previous component in the chain serving as the input to the next. This information could be incorporated with other routines to calculate parameters such as noise figure, gain/loss and attenuation in a similar fashion.

8.3 MCPA Design

Following on from the prediction tool development, a novel amplifier configuration has been presented which was shown to simultaneously improve upon linearity and efficency. The technique relied upon the use of a scaled version of the extracted envelope of the multi-tone signal to actively bias the amplifier. The technique has been shown to offer similar results as existing design methods but with the added advantage of having a relatively simplistic circuit.

The performance of this design has been demonstrated by comparison of worst-case adjacent channel IM_3 and amplifier efficiency with a normal biased circuit (a simple collector feedback circuit). The results show a significant improvement in both efficiency and linearity.

Due to the low level output level of the RF source the amplifier has been constructed with a feedback configuration so that a sufficiently high voltage level could be supplied to the detector circuitry. With a higher input power level a feedforward active biasing technique should offer a greater improvement in both linearity and efficiency. This is due to the fact that the feedback approach extracts the envelope from the RF output which includes the actual distortion effects of the amplifier.

As the performance of the active biasing technique relies largely on the ability to accurately extract the envelope of the multi-tone signal it is felt that any future enhancements to the circuitry should involve optimising the envelope detector section of the design.

References

[1] Ericsson Wireless Now, *Towards the Global Mobile Information Society. Whats it all about?*[0nline]. Available from:- http://www.demon.co.uk/aor/docs/IP3.htm [Acessed 4/4/98].

[2] Ericsson Wireless Now 2/98, *The global mobile Information Age* [online]. Available from: http://www.demon.co.uk/aor/docs/IP3.htm [Acessed 4/4/98].

[3] Bhawani Shankar, European Microwave Journal Staff, *Boundless Europe: The Wireless Revolution* [online]. Available from: http://www.mwjournal.com/IP3.htm [Acessed 4/4/98].

[4] I Brodsky, *The Wireless Revolution.*, New York: Van Nostrand Reinhold, 1980.

[5] H. Duncan, *MVDS market treds - a view from Europe*, Microwave Engineering Europe, July 1998, pp 27-32.

[6] Ericsson Wireless Now 2/98, *A Broad Look at Broadband* [online]. Available from: http://www.demon.co.uk/aor/docs/IP3.htm [Acessed 4/4/98].

[7] P.C. Yip, *High Frequency Circuit Design and Measurements.*, London: Chapman & Hall, 1991, pp 162-184.

[8] D.W. Bennett, R.J. Wilkinson, and P.B. Kenington, *Determining the Power Rating of a Multichannel Linear Amplifier*, IEEE Proc.-Commun., Vol. 142, No. 4, August 1995, pp 274-280.

[9] K.J. Parsons, R.J Wilkinson and P.B. Kenington, *A Highly-Efficient Linear Amplifier for Satellite and Cellular Applications.*, IEEE GLOBECOMM., 1995, pp 203-206.

[10] E. Ballesteros, F. Pérez, J. Pérez *Analysis and Design of Microwave Linearized Amplifiers using Active Feedback.*, IEEE Microwave and Guided Wave Letters, Vol. 36, No. 3, March 1988.

[11] S.C. Cripps, *Harmonic and Intermodulation Distortion in GaAsFET Amplifiers.*, Matcom Inc. Technical Note 2.1.

[12] D.D. Weiner and J.F. Spina, *Sinusoidal Analysis and Modeling of Weakly Nonlinear Circuits.*, New York: Van Nostrand Reinhold, 1980.

[13] G.A. Breed, *Test Setups for Measuring Intermodulation Distortion*, RF Design, August 1995, pp 60-66.

[14] L.E. Larson (Editor), *RF and Microwave Circuit Design for Wireless Communications*, Boston : Artech House, 1996, pp 382-395.

[15] K. Feher, *Digital Communications: Microwave Applications*, N.J. 07632: Prentice-Hall, 1981, pp 78-93.

[16] S.A. Mass, *Nonlinear Microwave Circuits.*, New York: IEEE Press, 1996.

[17] T.S. Laverghetta, *Handbook of Microwave Testing*, Artech House, Dedham, MA USA, 1981.

[18] M. Engelson, *Distortion Measurements Using the Spectrum Analyser*, RF Design, March 1995, pp 38-45.

[19] J. Thorpe, *Intermodulation testing in high performance receivers* [online]. Available from: http://www.demon.co.uk/aor/docs/IP3.htm [Acessed 1/1/98].

[20] J. Thorpe, *Intermodulation News - more IP3 thoughts and tests* [online]. Available from: http://www.demon.co.uk/aor/docs/jtimd.htm [Acessed 1/1/98].

[21] Anon., *Software Manual: Computer Boards CBI-488.2 GPIB Software*, Computer Boards, Inc.

[22] C. O Connor, *Vector Information Extraction from the Scalar Measurement of the Reflection Coefficient of a Device Under Test*, Masters Thesis, 1997.

[23] B.W. Kernighan, D.M. Ritchie, *The C Programming Language*, N.J. 07632: Prentice-Hall, 1988.

[24] S. Maas, *Nonlinear Analysis in RF Design*, RF Design, March 1995, pp 58-63.

[25] G. Rhyne, M. Steer, B. Bates *Frequency-Domain Nonlinear Circuit Analysis Using Generalised Power Series.*, IEEE Microwave and Guided Wave Letters, Vol. 36, No. 2, February 1988.

[26] V. Rizzoli, A. Neri, *State of the Art and Present Trends in Nonlinear Microwave CAD techniques.*, IEEE Microwave and Guided Wave Letters, Vol. 36, No. 2, February 1988.

[27] K. Kundert, A. Sangiovanni-Vincentelli, *Simulation of nonlinear circuits in the frequency domain.*, IEEE Trans. Computer-Aided Design, Vol. CAD-5, pp. 521-535, October 1986.

[28] J.H. Haywood, Y.L. Chow, *Intermodulation Distortion Analysis Using a Frequency-Domain Harmonic Balance Technique.*, IEEE Microwave and Guided Wave Letters, Vol. 36, No. 8, August 1988.

[29] V. Rizzoli *et al.*, *State-of-the-Art Harmonic-Balance Simulation of forced Nonlinear Circuits by the Piecewise Technique.*, IEEE Microwave and Guided Wave Letters, Vol. 40, No. 1, January 1992.

[30] S.A. Mass, *Third-order Intermodulation Distortion in Cascaded Stages.*, IEEE Microwave and Guided Wave Letters, Vol. 5, No. 6, July 1995.

[31] P.A. Sheridan, P.A. Perry, *Robust Nonlinear Multichannel Amplifier Characterisation.*, 28th European Microwave Conference Proceedings, Vol. 1, October 1998.

[32] K. Lu et al., *Low-Frequency Dispersion and its Influence on th Intermodulation Performance of AlGaAs/GaAs HBTs*, IEEE MTT-S Digest, 1996.

[33] Anon., *3G Market Overview and Technology Basics for cdma2000 and UTRA (ETSI W-CDMA)*, Hewlett Packard, 1998.